Lithium Manganese Spinel Cathodes for Lithium#Ion Batteries

Lithium Manganese Spinel Cathodes for Lithium-Ion Batteries

Yimeng Huang[1,†], Yanhao Dong[2,†], Sa Li[3], Jinhyuk Lee[2,4], Chao Wang[2], Zhi Zhu[2], Weijiang Xue[2], Yao Li[5,2], Ju Li[1,2,*]

[1]*Department of Materials Science and Engineering, Massachusetts Institute of Technology, Cambridge, MA, 02139, USA*

[2]*Department of Nuclear Science and Engineering, Massachusetts Institute of Technology, Cambridge, MA, 02139, USA*

[3]*Institute of New Energy for Vehicles, School of Materials Science & Engineering, Tongji University, Shanghai 201804, China*

[4]*Department of Mining and Materials Engineering, McGill University, Montreal, Quebec H3A 0C5, Canada*

[5]*State Key Lab of Metal Matrix Composites, Shanghai Jiao Tong University, Shanghai 200240, China*

*Corresponding authors. E-mail: liju@mit.edu (J. L.)

†Equal contribution.

Keywords: Lithium-ion batteries; Cathodes; Spinel; Degradation; High-rate electrodes

Abstract

Spinel $LiMn_2O_4$, whose electrochemical activity was first reported by Professor John B. Goodenough's group at Oxford in 1983, is an important cathode material for lithium-ion batteries, which attracts continuous academic and industrial interests. It is cheap and environmentally friendly, and has excellent rate performance with 3-dimensional (3D) Li^+ diffusion channels. However, it suffers from severe degradations, especially under extreme voltages and during high-temperature operations. In this review, the current understanding and future trends of the spinel cathode and its derivatives with cubic lattice symmetry ($LiNi_{0.5}Mn_{1.5}O_4$ that shows high-voltage stability, and Li-rich spinels that show reversible hybrid anion- and cation-redox activities) shall be discussed. Special attention is given to the degradation mechanisms, further development of spinel cathodes, and concepts of utilizing the cubic spinel structure to stabilize high-capacity layered cathodes and as robust framework for high-rate electrodes. "Good spinel" surface phases like $LiNi_{0.5}Mn_{1.5}O_4$ are distinguished from "bad spinel" surface phases like Mn_3O_4.

1. Introduction

Lithium-ion batteries (LIBs) have enjoyed great success in portable electronics and electric vehicles, and show considerable prospects in grid level energy storage. Such development dramatically accelerates the progress of modern civilization and is acknowledged by the 2019 Nobel Prize in Chemistry awarded to John B. Goodenough, M. Stanley Whittingham, and Akira Yoshino.[1] Among many other milestones that contributed to the huge success of LIBs is the development of three families of cathode materials (layered structure $LiCoO_2$,[2] spinel structure $LiMn_2O_4$[3] and olivine structure $LiFePO_4$[4]) pioneered by Goodenough and others. This review article shall focus on manganese spinel cathode $LiMn_2O_4$ and its derivatives, with cubic lattice symmetry on average.

The discovery of $LiMn_2O_4$ for battery applications came from the quest to find an inexpensive oxide as the cathode material.[5] In 1981, Hunter[6] first reported the conversion of spinel $LiMn_2O_4$ into a new form of manganese dioxide called λ-MnO_2 by chemical delithiation in aqueous acidic solutions. The λ-MnO_2 preserves the $[B_2]O_4$ framework of $A[B_2]O_4$ spinel and turns out to be the end product of $LiMn_2O_4$ after electrochemical delithiation. After early investigations of electrochemical lithiation of Fe_3O_4 spinel,[7] Thackeray *et al*. reported electrochemical lithiation[3a] and delithiation[3b] of $LiMn_2O_4$ spinel in 1983 and 1984, respectively, which boosted research interest in this family of cathodes with good thermal stability.[8] Further investigations of complex phase diagrams and versatile structure/chemistry of Mn-based materials[9] as well as efforts to optimize the electrochemical properties (especially on cycling)[10] led to the discovery and development of high-voltage spinel cathodes (e.g. $LiNi_{0.5}Mn_{1.5}O_4$[11]), high-capacity layered Li-/Mn-rich cathodes (e.g. Li_2MnO_3 and $xLiNi_{1/3}Co_{1/3}Mn_{1/3}O_2\cdot(1-x)Li_2MnO_3$[12]) and other advanced cathode materials/composites.[13] The major milestones of the development of $LiMn_2O_4$ and its derivatives are briefly summarized in the flow chart of **Figure 1**. To date, even though $LiMn_2O_4$ has smaller capacity and energy density compared to the later developed layered $LiNi_{1-x-y}Co_xMn_yO_2$ (NCM), $LiNi_{1-x-y}Co_xAl_yO_2$ (NCA), Li-/Mn-rich cathodes and $LiCoO_2$ (see comparison of different cathode materials in **Table 1**), it is cost-effective, non-toxic, and environmentally friendly (cobalt-free, with abundant non-toxic manganese) and has a more robust crystal structure with fast diffusion kinetics, so it is commonly blended with layered cathodes to reduce cost, increase structural and thermal stability, and improve rate performance.[14] High-voltage spinel $LiNi_{0.5}Mn_{1.5}O_4$ has promising energy density due to its high operating voltage at ~4.7 V vs. Li^+/Li. Also, the spinel structure is closely related to the layered and rocksalt structures of many LIB cathodes, and spinel-like structures can often be observed at the surface of degraded cathodes. And just like Li substitution of transition metals (TM) in layered compounds leads

to Li-rich cathodes with higher capacity due to the participation of oxygen redox, one may also create Li-rich spinels with reversible and/or irreversible hybrid anion- and cation-redox (HACR) activities.

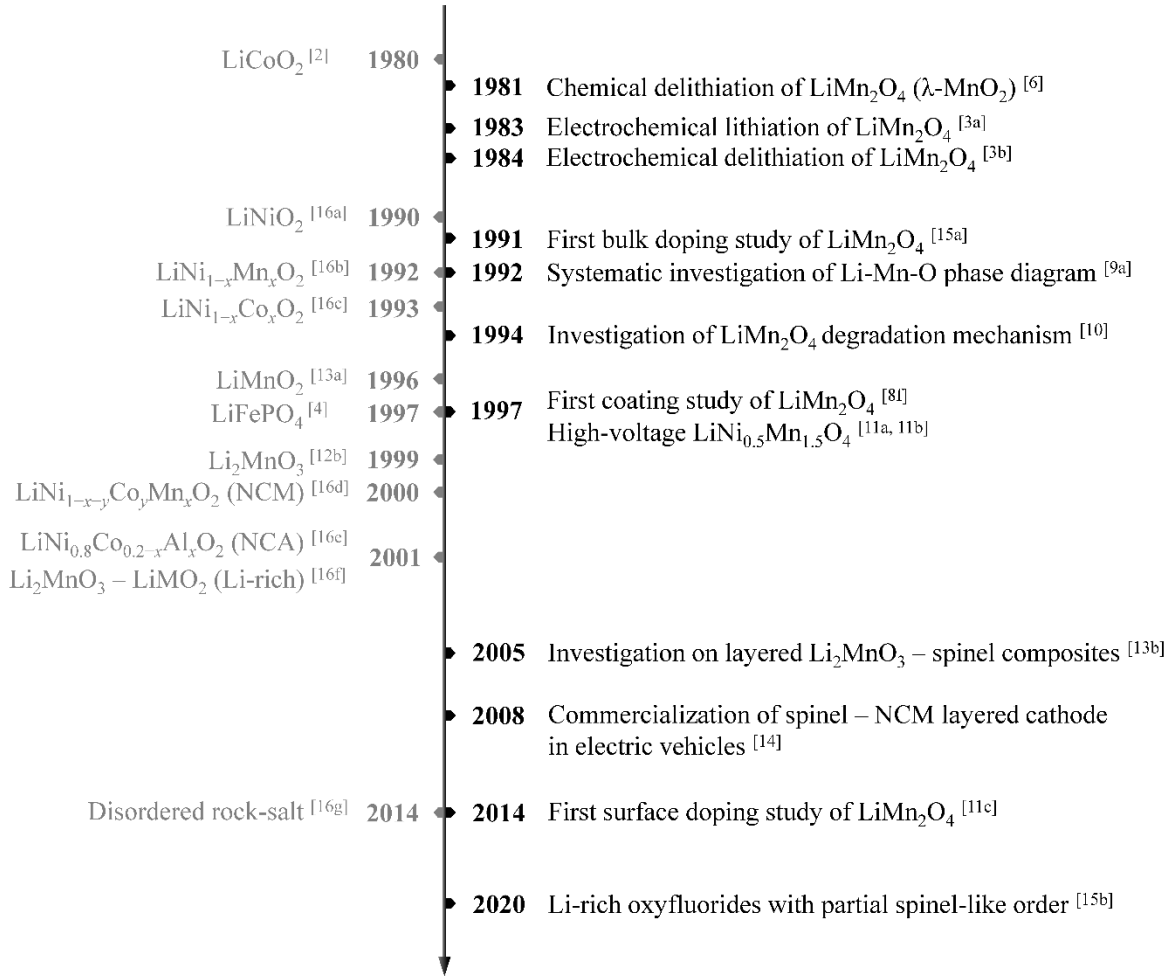

Figure 1. Development history of the spinel cathodes[3, 6, 8f, 9a, 10-11, 13b, 14-15] (right column) and the first studies of other major LIB cathodes (left column).[2, 4, 12b, 13a, 16]

Here we would like to make a distinction between "bad spinel" structures like the Co_3O_4 phase, where Li^+ diffusion channels are all blocked as both tetrahedral and octahedral sites are occupied by Co, and "good spinel" structures like $LiMn_2O_4$ and $LiNi_{0.5}Mn_{1.5}O_4$ where there are percolating 3D Li^+ diffusion channels. In this review we are mostly concerned with the latter, although on the surfaces of some layered compounds, "bad spinel" can also form, greatly

increasing the impedance. “Good spinel” surface phases, on the other hand, do not necessarily degrade the rate performance and can actually improve it.[17]

Past understanding and lessons learned from spinel cathodes could provide valuable insights and implications for future development of LIB cathodes in general. This review is organized as follows. Section 2 describes the fundamentals of spinel cathodes and its relation to layered and rocksalt lattice structures. Section 3 summarizes the understandings of their degradation mechanisms. Section 4 discusses degradation mitigation and future development strategies, including bulk doping, controlling dopant distribution (e.g., cation ordering and surface doping), coating, and development of novel liquid electrolytes and solid electrolytes. Section 5 discusses the stability of the spinel structure, summarizes the observations of spinel-like surface structures in degraded layered cathodes and discusses the integration of the spinel structure into the layered cathodes as structural stabilizer. Section 6 discusses the origin of fast kinetics in the spinel structure and the potential application of utilizing the spinel structure to design novel high-rate cathodes. Section 7 provides a conclusion with a summary of future directions for spinel cathodes.

Table 1. Comparison of common cathode materials in LIBs.

Material structure	Composition	Theoretical capacity [mAh/g]	Capacity at 0.1C [mAh/g] (voltage range)	Operating voltage vs. Li^+/Li [V]	Specific energy [Wh/kg]	Co/TM ratio	Cost	Refs.
Spinel	$LiMn_2O_4$	148	120 (3.0 – 4.3 V)	4.1	490	0	Low	[18]
	$LiNi_{0.5}Mn_{1.5}O_4$	147	125 (3.5 – 4.9 V)	4.7	590	0	Low	[19]
Layered	$LiCoO_2$	274	185 (3.0 – 4.45 V)	3.9	720	1	High	[20]
	$LiNi_{1/3}Co_{1/3}Mn_{1/3}O_2$	278	160 (2.8 – 4.3 V)	3.8	610	0.33	Medium	[21]
	$LiNi_{0.8}Co_{0.1}Mn_{0.1}O_2$	276	205 (2.8 – 4.3 V)	3.8	780	0.1	Medium	[21b, 22]
	$LiNi_{0.8}Co_{0.15}Al_{0.05}O_2$	279	200 (2.8 – 4.3 V)	3.8	760	0.15	Medium	[23]
	$Li_{1.2}Ni_{0.13}Co_{0.13}Mn_{0.54}O_2$	377	240 – 270 (2.0 – 4.8 V)	3.6	860 – 970	0.16	Medium	[24]
Olivine	$LiFePO_4$	170	150 (2.5 – 4.2 V)	3.4	510	0	Low	[25]
	$LiMn_{0.8}Fe_{0.2}PO_4$	171	160 (2.5 – 4.2 V)	4.1	650	0	Low	[26]

2. Fundamentals of $LiMn_2O_4$ and its derivatives

$LiMn_2O_4$ has a cubic spinel structure $A[B_2]O_4$ under the space group $Fd\bar{3}m$, where O anions form face-centered cubic (FCC) array at 32e (Wyckoff position), B-site Mn cations fill in 1/2 of the octahedral sites at 16d, and A-site Li cations fill in 1/8 of the tetrahedral sites at 8a. The 3D $[B_2]O_4$ array is formed by edge-sharing MnO_6 octahedra (**Figure 2a**), which offers a strongly bonded network for 3D Li^+ diffusion via the empty octahedral sites at 16c (**Figure 2b**). The LiO_4 tetrahedra centered at 8a sites are corner-shared with MnO_6 octahedra centered at 16d and face-shared with empty octahedra centered at 16c. This spinel structure (**Figure 3**, bottom panel) is closely related to the layered $Li(TM)O_2$ structure (**Figure 3**, top panel; which can also be viewed as an ordered rocksalt structure), both with the same FCC anion sublattice, but with different cation sublattice occupations. The layered compound $Li(TM)O_2$ obviously has a planar Li-TM-Li-TM cation concentration wave, with Li/(Li+TM) of 100% and 0% in the alternating layers, respectively, with an average TM valence of 3+. In contrast, the cubic spinel $Li(TM)_2O_4$ has Li/(Li+TM) occupation at 66.7% in one layer and 0% in the other layer,

with an average TM valence of 3.5+; furthermore, the 33.3% TM in the 66.7%-Li layer forms an ordered superlattice, imparting the system a cubic symmetry. The disordered rocksalt structure with the same chemical formula $Li(TM)O_2$ as the layered compound, on the other hand, destroys the planar Li-TM-Li-TM cation concentration wave altogether, and makes no distinction between layers, and there is only one cation sublattice with equal occupation of Li/TM. This also recovers the cubic symmetry on average, as shown in the middle panel of **Figure 3**. Li-rich disordered rocksalt structure materials $Li_{1+x}(TM)_{1-x}O_2$ are under investigation as high-capacity cathodes, as long as there is sufficient "Li-richness" x (beyond the ideal reference structure) to ensure Li conduction percolation.[16g] After sufficient delithiation (oxidation) of the layered compound $Li(TM)O_2$, phase transition from the layered structure in the top panel of **Figure 3** to the spinel structure in the bottom panel requires out-of-plane migration of 1/4 of the Mn in the TM layer to the octahedral sites in the Li layer, while Li ions are displaced from octahedral to tetrahedral sites. The similarities in anion lattice and cation occupancy relate many Mn-based spinel and layered compounds, as shall be discussed later. Tetrahedral-to-octahedral displacement of Li can take place when lithiating spinel $Li(TM)_2O_4$ to create average composition $Li_{1+x}(TM)_2O_4$ ($0 < x < 1$), which is a two-phase reaction (spinel to ordered tetragonal rocksalt compound $Li_2(TM)_2O_4$) that provides a flat voltage plateau below 3 V vs. Li^+/Li (**Figure 4**).[3a, 27] The lithiation of $LiMn_2O_4$ is charge-compensated by Mn^{4+}/Mn^{3+} redox couple, where $Li_{1+x}Mn_2O_4$ has $(1+x)$ Mn^{3+} and $(1-x)$ Mn^{4+} on average with $x > 0$. Because octahedral Mn^{3+} ($t_{2g}^3e_g^1$) is a Jahn-Teller ion while Mn^{4+} ($t_{2g}^3e_g^0$) is not, excessive Mn^{3+} (over 1/2 of total Mn) in $Li_{1+x}Mn_2O_4$ initiates cooperative Jahn-Teller distortion in the lattice and disrupts the cubic symmetry (to tetragonal), which degrades the material upon electrochemical cycling. On the other hand, for delithiation of $LiMn_2O_4$, cubic symmetry can be maintained throughout the entire range of $0 < y < 1$ in $Li_{1-y}Mn_2O_4$, offering better structural stability during cycling. Furthermore, Li occupies a diamond-like array at 8a sites with two sub-sets of

interpenetrating FCC Li patterns in $LiMn_2O_4$, where one ordered Li sub-set retains at $Li_{0.5}Mn_2O_4$ (y = 0.5) ideally. At this point, $LiMn_2O_4 \rightarrow Li_{0.5}Mn_2O_4$ would have given 74.1 mAh/g($LiMn_2O_4$) charge capacity, with the rest 74.1 mAh/g($LiMn_2O_4$) charge capacity from $Li_{0.5}Mn_2O_4 \rightarrow Li_0Mn_2O_4$ yet to come. Interestingly, Mn^{4+}/Mn^{3+} redox couple is very sensitive to Li^+ ordering, which leads to a small voltage step (~0.15 V) between two voltage plateaus around 4 V vs. Li^+/Li. This sensitivity also leads to a large voltage drop (> 1 V, **Figure 4**) between $LiMn_2O_4$ and $Li_{1+x}Mn_2O_4$ as it involves tetrahedral-to-octahedral Li sublattice shift, which practically limits the cycling of Li to only ~1 Li per two Mn from $[Mn_2]O_4$ to $Li[Mn_2]O_4$[27] in standard coarse-grained spinels.

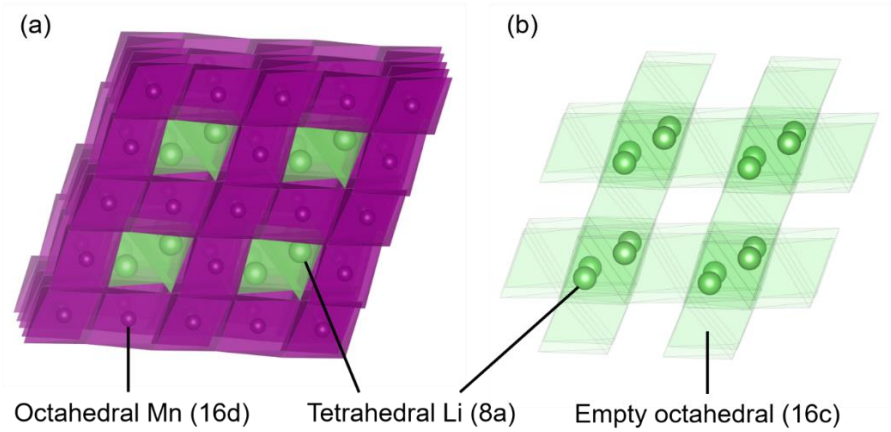

Figure 2. a) Crystal structure and b) Li^+ diffusion channel of $LiMn_2O_4$. Adapted from Ref. [28].

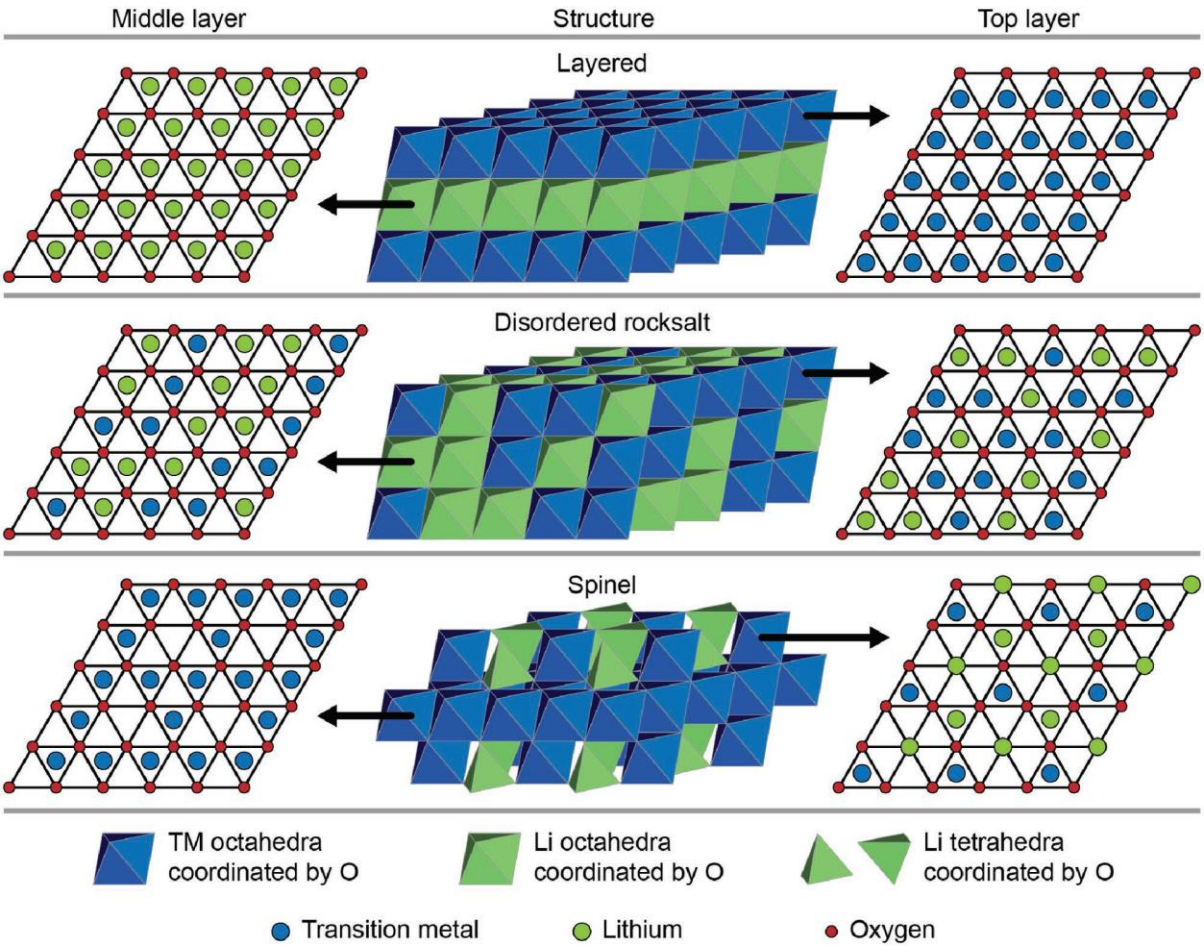

Figure 3. Schematic crystal structure and octahedral/tetrahedral site occupancy in layered (top panel), disordered rocksalt (middle panel) and spinel (bottom panel). Li occupancy is denoted by green circles/polyhedra. TM occupancy is denoted by blue circles/polyhedra. Different cation sizes and polyhedral distortions are omitted for simplicity. Reproduced with permission.[29] Copyright 2017, John Wiley & Sons, Inc.

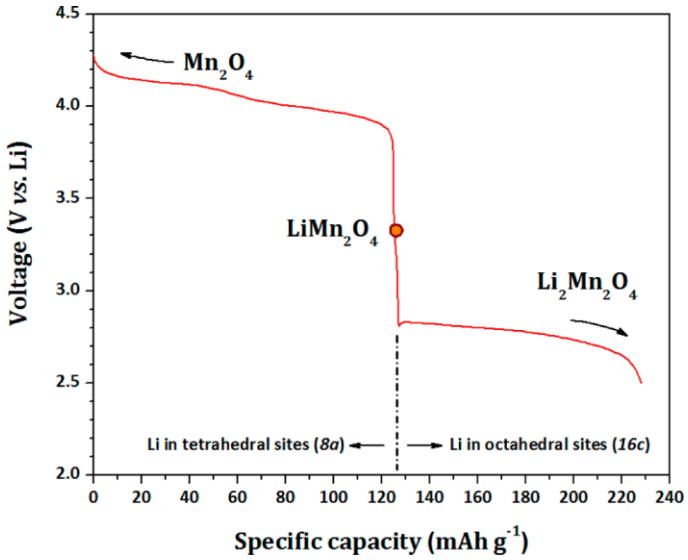

Figure 4. Voltage profile of $LiMn_2O_4$ during lithiation and delithiation. Reproduced with permission.[27] Copyright 2013, American Chemical Society.

$LiMn_2O_4$ has many derivatives that have similar chemistry and structures, indicated by many metastable compounds in Li-Mn-O phase diagrams constructed for either high-temperature synthesis or room-temperature chemical/electrochemical conversion.[9-10, 30] One useful phase diagram near the $LiMn_2O_4$ composition is shown in **Figure 5**, originally constructed by Thackeray *et al.*[9b, 10, 30a] to investigate the effect of composition and Mn valence on the electrochemical properties of spinel and spinel-related materials. Spinel materials with the greatest electrochemical interest lie on the "Spinel tie-line" connecting $LiMn_2O_4$ and $Li_4Mn_5O_{12}$ (equivalently $Li[Li_{1/3}Mn_{5/3}]O_4$), where Li substitutes up to 1/6 of the octahedral Mn with the chemical formula $Li_{1+x}Mn_{2-x}O_4$ (or $Li[Li_xMn_{2-x}]O_4$; $0 \leq x \leq 1/3$) while maintaining average cubic symmetry. Such "Li-rich spinel" $Li_{1+x}Mn_{2-x}O_4$ can be considered to be created by simultaneous lithiation and removal of Mn, which is not the same as pure lithiation, as is made clear by the different directions on the phase diagram in **Figure 5**. As mentioned above, pure lithiation of $LiMn_2O_4$ (along the dashed line from $LiMn_2O_4$ to the end product $Li_2Mn_2O_4$ = $LiMnO_2$, which can be rocksalt or layered) often triggers a spinel-to-

ordered tetragonal rocksalt phase transition due to reduced Mn valence (too much Mn^{3+} makes the system prone to Jahn-Teller distortion), while its delithiation (along the dashed line from $LiMn_2O_4$ to the end product λ-MnO_2) follows a solid-solution behavior. Similar trends apply to Li-rich spinel $Li_{1+x}Mn_{2-x}O_4$, where further lithiation enters the two-phase regime, and delithiation enters the cubic defect-spinel regime ($LiMn_2O_4$ - $Li_4Mn_5O_{12}$ - λ-MnO_2 triangle). Accompanied with Li substitution $Li_{1+x}Mn_{2-x}O_4$ (i.e. $Li[Li_xMn_{2-x}]O_4$) is the increase of average Mn valence to $(7-x)/(2-x)$, so that Mn^{4+}/Mn^{3+} redox couple can only provide $(1-3x)/(2-x)$ electrons per Mn and charge-compensate the removal of $(1-3x)$ Li ions. Therefore, the Mn^{4+}/Mn^{3+} cation-redox capacity (proportional to the total length of the dashed line passing through the spinel composition in **Figure 5**) decreases with increasing Li-richness x. This means if a Li-rich spinel (an extreme case would be x=1/3 or $Li_4Mn_5O_{12}$ where 100% of Mn valence is 4+) can still give significant charging capacity experimentally[31], then part of this capacity must originate from oxygen redox, or hybrid anion- and cation-redox (HACR) activities[32]. On the other hand, the increase of average Mn valence broadens the cubic spinel regime of $Li_{1+x}Mn_{2-x}O_4$ before transforming to tetragonal rocksalt phase, and also lowers the average Mn valance to $(6-x)/(2-x)$ in fully lithiated product $Li_{2+x}Mn_{2-x}O_4$. The latter decreases c/a ratio in tetragonal rocksalt $Li_{2+x}Mn_{2-x}O_4$, e.g. from average valence of +3 and c/a = 1.16 in $Li_2Mn_2O_4$ to +3.4 and c/a = 1.11 in $Li_7Mn_5O_{12}$, which reduces the damaging Jahn-Teller effect.

Because of the versatile valence, stoichiometry and polymorphism that Li-Mn-O based compounds can adopt, the obtained phases strongly depend on synthesis methods and conditions.[30] For example, while $LiMn_2O_4$ is typically synthesized at higher temperatures > 800 °C, $Li_4Mn_5O_{12}$ often forms at lower temperatures around 400 °C, and may result in impurity phases with other Li/Mn ratios; $LiMnO_2$ can have various crystal structures of rocksalt (tetragonal), layered (monoclinic), staggered configurations (orthorhombic) and their composites.[3a, 13a, 30a, 33] The last and probably the most important derivative of $LiMn_2O_4$ is the

high-voltage spinel $LiNi_{0.5}Mn_{1.5}O_4$, where Ni^{2+} substitution sets all Mn in +4 valence. It operates on Ni^{4+}/Ni^{2+} double redox at ~4.7 V vs. Li^+/Li, with a theoretical capacity of 147 mAh/g and a practical capacity of 125 mAh/g.[19] Because of the higher energy density and improved cycling stability, $LiNi_{0.5}Mn_{1.5}O_4$ has attracted continuous interest since its first reports in 1997.[11a, 11b]

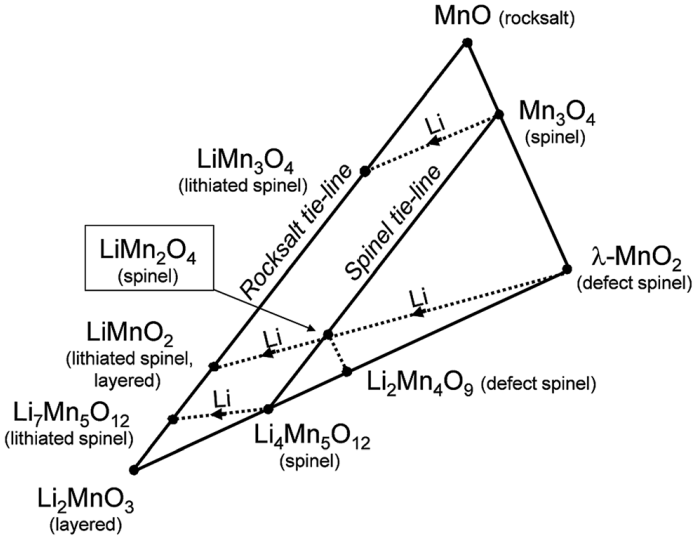

Figure 5. Li-Mn-O phase diagram near $LiMn_2O_4$ composition. Reproduced with permission.[30a] Copyright 2018, Royal Society of Chemistry.

3. Degradation mechanisms of spinel cathodes

An ideal electrode for LIBs should be a partially closed system that only allows the removal and insertion of Li via ambipolar diffusion of Li^+ and electrons. It generally does not apply to real materials as side reactions take place at the interface between active electrode materials and organic liquid electrolytes, where there are often effluences of TMs and oxygen, especially at extreme potentials. The resultant solid products form a passivation layer between electrodes and electrolytes, known as solid-electrolyte interphases (SEIs) at the anode side and cathode-electrolyte interphases (CEIs) at the cathode side.[34] Gaseous products could evolve mainly in the form of O_2, CO_2 and others, as observed in differential electrochemical mass spectrometry (DEMS) measurements of charged cathodes and some anodes (e.g. $Li_4Ti_5O_{12}$).[35] These

soluble products could enter the liquid electrolyte, e.g. the well-known problem of TM dissolution for $LiMn_2O_4$ and other Mn-based cathodes.[36] This is an important issue, not only because it leads to the loss of active cathode materials, but also because the dissolved TM ions can migrate to the anode side under electric field and/or concentration gradient and deposit on the anode surface under a low potential (vs. Li metal, and thus a reducing condition), as confirmed by various experimental techniques (e.g. energy-dispersive X-ray spectroscopy (EDX),[37] Rutherford backscattering spectroscopy (RBS),[8d] secondary ion mass spectrometry (SIMS),[38] X-ray photoelectron spectroscopy (XPS),[8d, 37b] and X-ray absorption near edge spectroscopy (XANES)[39]). The deposited TMs are known to affect the SEI of graphite anodes that significantly degrades the battery,[11c, 37a, 40] and change the deposition/growth morphology of Li metal anodes[41] that are under intense development currently.[42] The problem of TM dissolution is arguably the Achilles' Heel of $LiMn_2O_4$ and has been attracting continuous research interests over decades.

Before LIBs, Mn dissolution of $LiMn_2O_4$ was investigated by Hunter[6] in aqueous acidic solutions, which produced Li^+ and Mn^{2+} in the solution and λ-MnO_2 (with all Mn being +4 valence) at room temperature. Based on this observation, Hunter proposed a conversion reaction:

$$2LiMn_2O_4 = Li_2O + 3MnO_2 + MnO \quad (1)$$

where Li_2O and MnO are soluble under acidic conditions, based on a disproportionation mechanism:

$$2Mn^{3+} = Mn^{2+} + Mn^{4+} \quad (2)$$

at the surface. Outward ambipolar diffusion of Li^+ and electron polarons (**Figure 6**) then follows, until the bulk is turned into λ-MnO_2. This mechanism was followed and extended by Thackeray *et al.*[3b] in their first report of electrochemical delithiation of $LiMn_2O_4$, which proved both Li^+ and electron polarons have sufficiently high lattice diffusivity at room

temperature and modified the disproportionation mechanism by assigning different surface and bulk stabilities (denoted as subscripts) of $Mn^{2+/3+/4+}$:

$$(Mn^{3+})_{Surface} + (Mn^{3+})_{Bulk} = (Mn^{2+})_{Surface} + (Mn^{4+})_{Bulk} \quad (3)$$

This mechanism is supported by the observations of Mn^{2+} in aqueous solutions[6] and organic electrolytes (by differential pulse polarography[43] and X-ray absorption near-edge structure spectra[44]), and is consistent with the observations that Mn dissolution becomes more severe with smaller particles and larger specific surface areas, higher acidity of the electrolyte, and higher temperatures.[3b, 6, 45] (There are two recent studies that reported Mn^{3+} as the main TM dissolution species of $LiMn_2O_4$ in battery electrolytes, while Mn^{2+} still being the main dissolution species of $LiNi_{0.5}Mn_{1.5}O_4$.[46] The investigation was followed by Hanf *et al*.[47] showing that Mn^{3+} is the main product of $LiNi_{0.5}Mn_{1.5}O_4$ in aqueous acidic solutions, while Mn^{2+} dominates in organic electrolytes.) Therefore, this disproportionation mechanism has been widely stated and discussed in the literature. However, it requires caution to treat Mn^{3+} disproportionation as the only cause of Mn dissolution. This is because if this mechanism dominates, Mn dissolution would be more pronounced as Mn valence decreases (which peaks at the lowest voltage at the end of discharge/lithiation) and less so as Mn valence becomes higher (which should cease at the highest voltage at the end of charge/delithiation); however, it has been shown by various experiments that Mn dissolution accelerates both in discharged states < 3.1 V vs. Li^+/Li and in charged states > 4.1 V, and peaks at the highest voltage during charge.[43-45] The disproportionation argument again fails in $LiNi_{0.5}Mn_{1.5}O_4$, where all Mn are at +4 valence, yet Mn dissolution still takes place (albeit less than $LiMn_2O_4$) and accelerates at higher charge voltages.[40] The observed Mn dissolution under highly charged states indicates the surface instability of highly-delithiated $LiMn_2O_4$ and $LiNi_{0.5}Mn_{1.5}O_4$, which could result in anion-redox induced global oxygen mobility[32], oxygen loss, TM reduction and side reactions with the organic electrolytes. For example, with combined XPS, electron energy loss

spectroscopy (EELS), scanning transmission electron microscopy (STEM), and density functional theory (DFT) calculations, Tang *et al*.[48] reported the reduction of surface Mn upon charging and oxidation of surface Mn upon discharging, which is contrary to what are expected in the bulk; Gao *et al*.[49] used atomic-level STEM to directly characterize and visualize oxygen loss, Mn reduction and surface reconstruction upon charging; using epitaxial $LiMn_2O_4$ thin films, Hirayama *et al*.[50] showed surface instability/reconstruction and Mn dissolution are surface dependent and more pronounced at (110) than at (111) surface. These observations have shed light on the fundamental mechanism of high-voltage instability of spinel cathodes, especially at the surface.[51] Conventionally, such surface instability was thought to be only applicable to redox couples that are pinned at the top of O-2*p* bands, e.g. Co^{4+}/Co^{3+} redox couple in $LiCoO_2$. But as is clear in the example of $LiMn_2O_4$, the pinning could be stronger at the surface than in the bulk, and surface oxygen loss accompanied by TM reduction and surface reconstruction should be general in most of the high-voltage cathode materials. The as-reduced TMs can lead to surface phase transformation, and in the case of $LiMn_2O_4$ and other Mn-based cathodes, TM dissolution in the form of Mn^{2+}.

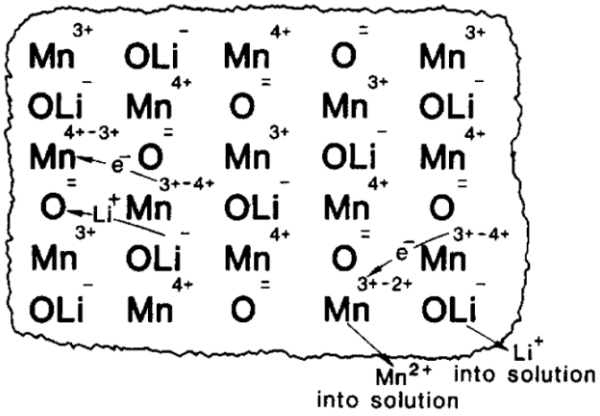

Figure 6. Schematic mechanism of the conversion of $LiMn_2O_4$ to λ-MnO_2 in aqueous acidic solutions. Reproduced with permission.[6] Copyright 1981, Elsevier Inc.

Beyond TM dissolution that causes loss of active cathode materials, there is also surface phase transformations that increase the impedance of cathodes.[52] Both factors contribute to capacity decay and quantitatively, the loss of active materials was found to be only responsible for 20-30% of the overall capacity decay.[43] The impedance growth is attributed to surface phase transformation with poor Li^+ diffusivity, which happens at both ends of charge and discharge, especially under fast charging/discharging, non-equilibrium conditions and after prolonged cycling. At the end of discharge, the damaging Jahn-Teller distortion[53] could initiate at the surface and induce cubic-to-tetragonal phase transformation, where ordered tetragonal rocksalt $Li_2Mn_2O_4$ phase was observed at the surface of $LiMn_2O_4$ cycled between 3.3 – 4.2 V vs. Li^+/Li.[54] At the end of charge, on the other hand, oxygen escape leads to the formation of Mn_3O_4 (with average Mn valence of +8/3, less than +3) phase at the surface, which produces soluble Mn^{2+}.[48] Such electrochemically induced phase transformations were recently investigated by Liu *et al*.[55] via advance characterizations of combining *in situ* synchrotron high-resolution X-ray diffraction (XRD), X-ray absorption spectroscopy (XAS), X-ray fluorescence (XRF) and STEM. The results (**Figure 7**) clearly reveal the formation of Mn_3O_4 at upper charge voltage of 4.3 V vs. Li^+/Li and the formation of $Li_2Mn_2O_4$ at lower discharge voltage of 3.4 V vs. Li^+/Li. The phase transformations are partially irreversible and lead to particle cracking upon cycling, which further causes detrimental increase in reactive surface area. Similar observations of Mn_3O_4-like structures ("bad spinel") have also been reported by Lin *et al*.[56] on the surface (about 2 nm thick) of $LiNi_{0.5}Mn_{1.5}O_4$ during the first charge up to 4.9 V vs. Li^+/Li, whereas a rocksalt-like structure was observed in the sub-surface region. Interestingly, it was shown by Amos *et al*.[57] by aberration-corrected STEM that the surface of uncycled $LiMn_2O_4$ can automatically reconstruct into a thin surface layer of Mn_3O_4 ("bad spinel", which is also electrolyte soluble) and a sub-surface layer of $Li_{1+x}Mn_2O_4$ near the surface of a bulk $LiMn_2O_4$ particle (**Figure 8**), which indicates a surface oxygen deficiency

and a subsequent disproportionation reaction. The blockage of the 3D Li^+ diffusion channel in Mn_3O_4-like and rocksalt-like structures is likely to be the reason why the transformed phases dramatically increase cell impedance.

The observed TM dissolution, oxygen escape, surface reconstruction and surface phase transitions point to the critical role of the interactions between the cathode surface and the electrolyte under dynamic conditions, which are still not well understood at the present stage. On one hand, surface structure and chemistry of the spinel cathodes need to be better characterized and studied, as a function of crystal orientations, terminating species, segregating cations and electrochemical potentials. Special attention should be paid to the surface phase stability and diffusion kinetics of Li^+ and TM species in pristine and transformed surface structures. In addition to various advanced experimental tools, first-principles calculations should help to construct a database and offer mechanistic insights. For example, stability and phase diagram of $LiMn_2O_4$ (001) and (111) surfaces have been evaluated and constructed by Kim *et al*.[58] using DFT calculations with different terminations and at various chemical potentials of lithium, which suggests (111) surfaces with Li-rich surface layers are more resistant to Mn dissolution than (001) surfaces. Ti and Ta surface doping have been shown by DFT calculations to promote the formation of rocksalt phase, lower Ni valence under fully charged state, and stabilize the oxygen framework of $LiNi_{0.5}Mn_{1.5}O_4$, which suggests suppressed side reactions and oxygen evolution during electrochemical cycling.[59] Such simulations would offer valuable insights to the experimental design of particle morphology, surface composition and others. On the other hand, it is more challenging to understand the complicated interactions at the solid-liquid interface during electrochemical cycling, especially the formation and dynamic evolution of CEIs, decomposition and oxidation of organic electrolytes, and surface diffusion, solvation and dissolution of Mn and other TM species. It again requires synergetic efforts with various *ex situ* and *in situ* characterization tools (e.g.,

time-of-flight secondary-ion mass spectroscopy (TOF-SIMS)[60] and ultraviolet-visible spectroscopy[61] and advanced simulation techniques (e.g., *ab initio* molecular dynamics (AIMD) simulations[61-62]) to capture and understand the underlying thermodynamics and dynamics, which could help to design stable artificial CEIs, novel electrolytes and additives to fully solve the TM dissolution problem. Such mechanistic understandings hold the key for the future development of spinel cathodes.

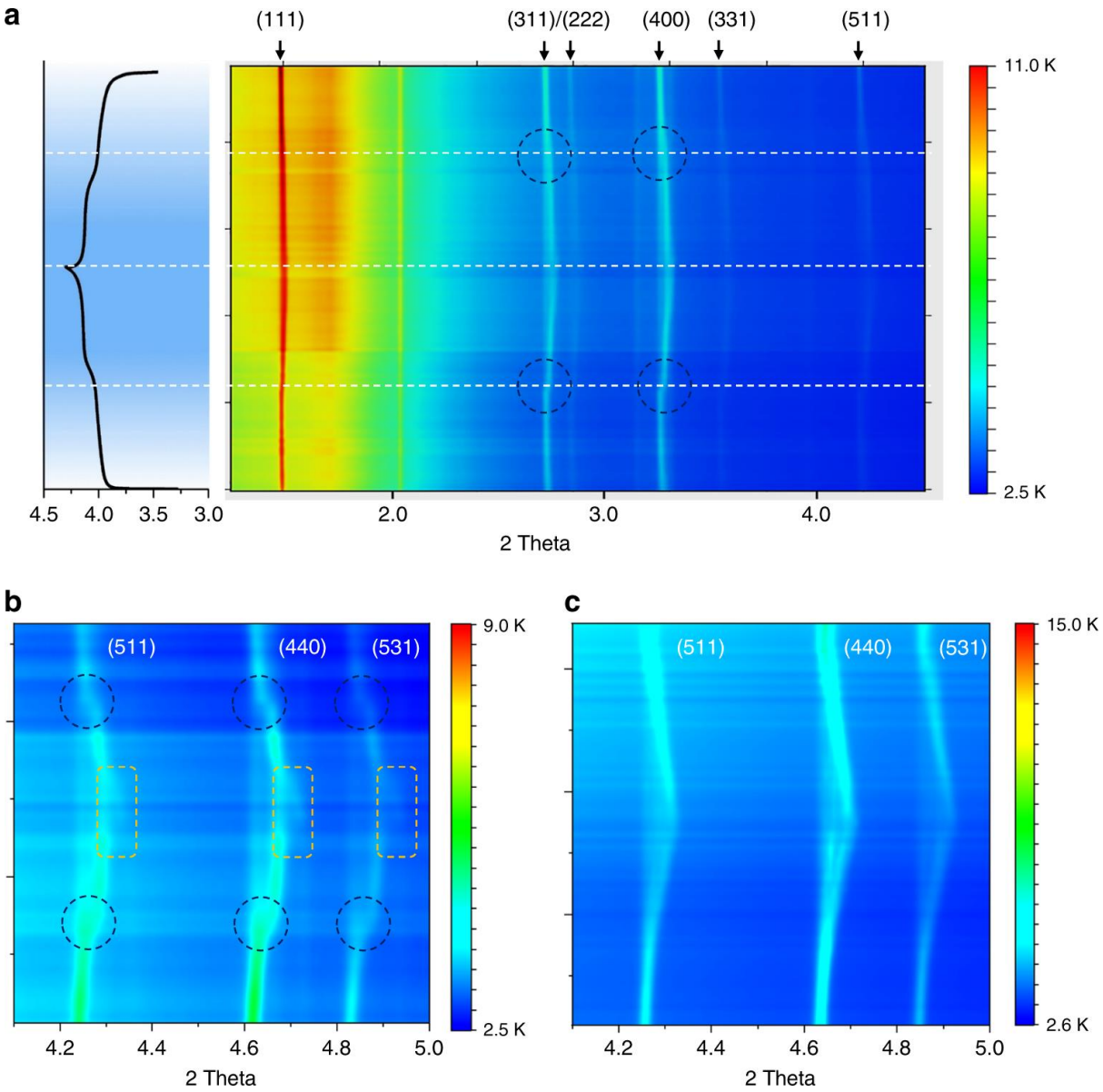

Figure 7. a) *In situ* synchrotron high-resolution X-ray diffraction of $LiMn_2O_4$ for the first charge and discharge between 3.4 and 4.3 V vs. Li^+/Li. b) Enlarged view of (a). c) Enlarged view of similar measurements performed on $Li_{1.1}Mn_{1.9}O_4$ for the first charge and discharge

between 3.4 and 4.3 V vs. Li^+/Li. Reproduced with permission.[55] Copyright 2019, Springer Nature.

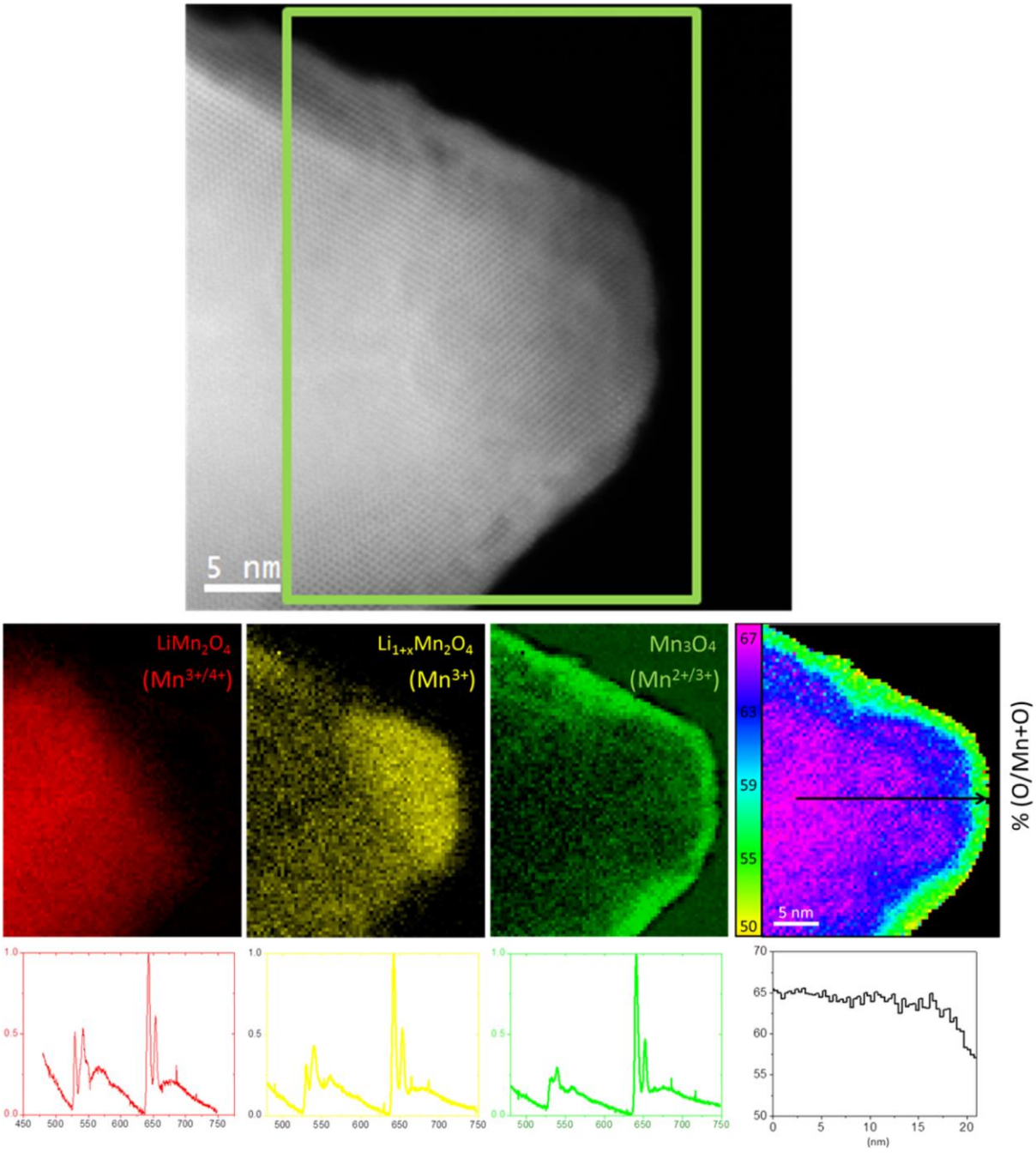

Figure 8. High-angle annular dark-field imaging (HAADF) STEM image of a $LiMn_2O_4$ particle, with green rectangle showing the inspected area (top panel). Colored maps (red, yellow and green) and corresponding EELS spectra (in the same color) representing the location of different Mn valence states, and a map showing atomic ratio of O/(Mn+O)

calculated from the O K edge and Mn $L_{2,3}$ edge (middle and bottom panels). Reproduced with permission.[57] Copyright 2016, American Chemical Society.

4. Future development of spinel cathodes

Because of the above issues of TM dissolution and surface phase transformations, spinel cathodes suffer from severe degradation especially during high-temperature cycling (e.g., at 50 ^{o}C), and there have been tremendous efforts to improve cycling and rate performance. First of all, bulk doping is the most practiced method. For $LiMn_2O_4$, considering the disproportionation mechanism of Mn^{3+}, it is beneficial to increase the average Mn valence, which is possible by lower-valence (less than or equal to +3) cation doping. Many dopants (including Li^{+}, Mg^{2+}, Zn^{2+}, Ni^{2+}, Co^{2+}, Cr^{2+}, Cu^{2+}, Al^{3+}, Fe^{3+} and Sc^{3+})[10, 55, 63] have been reported to improve cycling properties of $LiMn_2O_4$, among which doping with slightly excess Li is one of simplest and most efficient method. Note that Li richness improves cycling at the expense of the available Mn^{4+}/Mn^{3+} cation-redox capacity, and thus lowering the cation-redox capacity. The anion-redox capacity would need to be activated at higher charging voltages. Such a trade-off needs to be considered in stabilizing $LiMn_2O_4$. Meanwhile, successful dual- and multi-cation doping strategies have been reported, which opens a larger compositional space for optimizations that could be assisted by machine learning.[64] For example, Xiong *et al*.[63f] recently reported $Cu^{2+}/Al^{3+}/Ti^{4+}$ multi-cation doping has a synergetic effect to improve the cycling stability of $LiMn_2O_4$. Meanwhile, higher-valence (above +3) cation doping (e.g. Ti^{4+})[63c, 63d] and anion substitution with F^{-}[63e, 65] were also reported to improve the cycling of $LiMn_2O_4$. This seems counter-intuitive at first glance as they would lower Mn valence, hence should not be beneficial. Nevertheless, their effectiveness suggests the complicated role of doping atoms most likely in the surface structure and chemistry, which is worthwhile for future studies especially via advanced experimental and simulation techniques. On the other hand, doping with

electrochemically active elements led to the development of $LiNi_{0.5}Mn_{1.5}O_4$, where Ni^{2+} sets all Mn at +4 valence that makes the structure stable. Albeit with similar capacity, $LiNi_{0.5}Mn_{1.5}O_4$ has higher energy density (because $Ni^{4+/2+}$ operates at a higher redox potential at ~4.7 V vs. Li^+/Li without sacrificing capacity[66]) and better cathode stability than $LiMn_2O_4$. However, the large-scale application of $LiNi_{0.5}Mn_{1.5}O_4$ is hindered by the obstacle to commercialize a stable 5 V electrolyte. Nevertheless, the intrinsic high-voltage stability of $LiNi_{0.5}Mn_{1.5}O_4$ also leads to various doping studies, including Mg^{2+}, Fe^{3+}, Co^{3+}, Cr^{3+}, Al^{3+} and Ru^{4+}, to further increase cycling performance.[67] A recent work by Liang *et al*.[67a] explored site-selective Mg doping in both tetrahedral (8a) and octahedral (16c) sites and demonstrated excellent cycling stability with 86% capacity retention after 1500 cycles at 1 C and 87% capacity retention after 2200 cycles at 10 C. Furthermore, engineering the oxygen stoichiometry was explored in spinel cathodes.[8c, 8d] Considering the complicated Li-Mn-O phase diagram and the sensitivity on synthesis condition and methods, precise control of the oxygen stoichiometry and defects may be challenging, but may also provide new opportunities in novel phases and/or composites with good properties.

Second, in addition to bulk doping, it is also important to tailor the dopant distributions. It was well recognized that in $LiNi_{0.5}Mn_{1.5}O_4$, different level of Ni/Mn cation ordering (controllable by synthesis conditions) gives rise to variations in capacity and cycling stability.[68] Such cation ordering in the bulk lattice originates from strong cation-cation interactions and would be smeared out with larger contributions of configuration entropy. Therefore, it should be general in many other heavily doped spinel cathodes, especially for the dopants with very different size and charge, strong magnetic interactions, and when using low temperature synthesis methods. This ordering phenomenon is worthwhile to be studied in the future, especially its influence on electrochemical properties. Apart from dopant distributions in the bulk, surface doping is now recognized as an efficient method to stabilize spinel cathodes,

as the capacity is minimally affected by the trace amounts of electrochemically inactive dopants.[69] This strategy was first reported by Lu *et al*.,[69a] where a thin layer of TiO_2 was coated on the surface of $LiMn_2O_4$ via atomic layer deposition (ALD) or sol-gel method followed by heat treatment. The obtained Ti surface-doped $LiMn_2O_4$ showed improved cycling with suppressed Mn dissolution and less impedance growth. A recent progress has been made by Piao *et al*.,[69b] where site-selective (occupying empty 16c octahedral site) Al surface doping can dramatically improve cycling (97.6% capacity retention after 150 cycles at 0.1 C) and rate performance of $LiNi_{0.5}Mn_{1.5}O_4$. The surface doping approach could be obtained by two ways: from the kinetic perspective, one can uniformly coat the cathode particles by wet-chemistry or vapor-deposition methods, followed by a low-temperature and/or short-time annealing to suppress long-range cation diffusion; from the thermodynamic perspective, one can use dopant elements that tend to segregate at the surface. We believe this promising approach would lead to fruitful results in the future development of spinel cathodes.

Third, surface coating is another commonly practiced method to improve cycling performance, with a wide range of coating materials, including oxides (e.g. Li_2O:B_2O_3, Al_2O_3, ZrO_2, ZnO, SiO_2, Li_2ZrO_3, and $LiNi_{1-x}Co_xO_2$)[8f, 70], fluorides (e.g. AlF_3)[71], phosphates[72] (e.g. $Li_3V_2(PO_4)_3$[73]) and polymers[74]. With recent development in solid electrolytes for LIBs, coating spinel cathodes with fast Li^+ conductors such as $Li_{6.4}La_3Al_{0.2}Zr_2O_{12}$ has also attracted attention.[75] Typically, the coating layer can physically separate the contact between active cathode materials and organic electrolytes and suppress side reactions such as Mn dissolution. In other words, it should be less reactive and catalytically inactive to the electrolytes than the spinel cathodes under dynamic conditions. Meanwhile, it should have a minimal effect on the impedance, with the ideal one having a good lattice match with spinel cathodes and being a good Li^+ and electronic conductor. Moreover, it is important to achieve uniform thin coating with good wetting properties, which remains conformal and all-covering not only in the pristine

state but also during electrochemical cycling. Therefore, despite of much progress that has been achieved, more investigations on new materials and scalable cost-effective synthesis methods are required to optimize the coating of spinel cathodes.

Forth, the morphology of spinel cathodes can be tuned to improve cycling. While nanomaterials[76] are attractive due to short diffusion length, good stress relief and damage tolerance, and other intriguing properties, coarse-grained $LiMn_2O_4$ with smaller specific surface area hence less side reactions is more desirable in terms of cycling stability. The particle size effect on Mn dissolution was observed in Hunter's experiments and later discussed by Thackeray *et al*.[3b, 6] Previous experimental and simulation results also suggest different stability and Mn dissolution rates at surfaces with different surface inclinations, so it could be beneficial to control the shape and crystal orientation of the particles. This could be achieved by molten salt method and tuned by different liquid-solid interfacial interactions during high-temperature synthesis. Since the low-cost solid-state synthesis is the preferred route for large-scale production, the interplay among particle size, dispersion, crystallinity and electrochemical properties should be also tailored by adjusting the heat-treatment schedule and different precursors/raw materials. Such a knowledge of know-how is a non-trivial issue that deserves detailed studies and optimizations, probably with the aid of the recently developed machine learning and high throughput strategies. Meanwhile, different synthesis methods and heat-treatment processes would influence defects (e.g., oxygen vacancy) and cation ordering, which should be considered to separate the processing and chemical effects on the electrochemical performances.

Fifth, modifications of the organic liquid electrolytes could be beneficial. Previous studies in $LiMn_2O_4$ have shown that additives such as $(CH_3)_3SiNHSi(CH_3)_3$, LiBOB, $CaCO_3$ and pyridine could help improve cycling, either due to the formation of a more stable surface phase or through scavenging the damaging HF in the organic electrolytes.[77] Meanwhile, advanced

liquid electrolytes for LIBs and other aqueous/non-aqueous batteries are under rapid development in recent years.[78] For example, Chen *et al*.[79] reported stable cycling of $LiMn_2O_4$ cathodes (paired with $Li_4Ti_5O_{12}$ anodes) in 2.5 V aqueous LIBs using super-concentrated aqueous electrolytes. For $LiNi_{0.5}Mn_{1.5}O_4$, Suo *et al*.[80] recently reported a class of full-fluoride electrolyte that enables highly stable 5-V-class lithium metal batteries, demonstrating > 130 cycles at 0.36 C with slightly excess (1.4×) lithium as the anode and a high-loading $LiNi_{0.5}Mn_{1.5}O_4$ cathode (14.7 mg/cm^2, 1.83 mAh/cm^2). Note that the development of advanced electrolytes and additives for $LiMn_2O_4$ is relatively less explored compared to the extensively practiced doping and coating strategies, and commercialization of $LiNi_{0.5}Mn_{1.5}O_4$ is also hindered by the lack of high-performance 5 V electrolyte. Therefore, there is plenty of room for the development of novel electrolytes, which may provide a good solution for spinel cathodes, including the challenging problem of high-temperature cycling.[81]

Lastly, the application of spinel cathodes in all-solid-state batteries could be a by-pass solution to the TM dissolution problem in liquid electrolytes. Some solid electrolytes are kinetically stable at 5 V vs. Li^+/Li, which could enable the use of $LiNi_{0.5}Mn_{1.5}O_4$. Spinel cathodes with cubic symmetry, 3D diffusion channel, and isotropic chemical expansion during electrochemical cycling also fit well with solid electrolytes. Preliminary results in the literature have reported successful usage of $LiMn_2O_4$ and $LiNi_{0.5}Mn_{1.5}O_4$ in bulk-type all-solid-state batteries with solid polymer electrolytes (e.g., polyoxyethylene-based[82] and polycarbonate-based polymer electrolytes[83]), sulfide-based solid electrolytes (e.g., $Li_2S–P_2S_5$[84] and $Li_{10}GeP_2S_{12}$[85]), and oxide-based solid electrolytes (e.g., $Li_{1.4}Al_{0.4}Ti_{1.6}(PO_4)_3$[86]), as well as thin-film-type all-solid-state batteries (with LiPON[87] and $Li_{0.17}La_{0.61}TiO_3$[88] solid electrolytes). Note that there are many more reports on full cells using solid polymer electrolytes than using sulfide-based solid electrolytes, and there are few reports on full cells using oxide-based solid electrolytes, which suggest challenges in processing all-solid-state

batteries with inorganic electrolytes, especially oxides. It also implies that even though oxide-based electrolytes such as garnet-structure $Li_7La_3Zr_2O_{12}$ (LLZO) has higher modulus (which is argued to be able to suppress lithium dendrite penetration) and larger stability voltage window, how to process them remains a great challenge. The high-temperature sintering process also raises the interdiffusion problem and potential formation of impurity phases, which have been reported in the literature.[86a, 89] Another important challenge is the interfacial stability between spinel cathodes and solid electrolytes during electrochemical cycling, including wetting and contact, chemical compatibility, and electrochemical stability. Coating of spinel cathodes may still be necessary to address the interfacial problem. For example, amorphous $Li_4Ti_5O_{12}$ and Li_3PO_4 thin-film coatings were reported to improve the electrochemical performance of $LiMn_2O_4$ and $LiNi_{0.5}Mn_{1.5}O_4$ in all-solid-state batteries, respectively.[84b, 84c] For high-rate applications that require high power density and/or fast charging, even though spinel cathodes have good diffusion kinetics, most solid electrolytes have limited critical current density, beyond which fast electrolyte degradation and shorting would occur. Therefore, more development in the processing technique, interfacial stability, coatings and solid electrolytes are required to achieve practical applications of spinel cathodes in advanced all-solid-state batteries.

5. Spinel structure as degradation product and structural stabilizer for layered cathodes

While the above content focuses on spinel cathodes, particularly on $LiMn_2O_4$ and $LiNi_{0.5}Mn_{1.5}O_4$, below we will discuss how stability and high rate performance of the spinel structure could help to design better LIB cathodes. This section focuses on the stability of the spinel structure that justifies its presence in various degraded layered cathodes and how it is integrated into layered cathodes to improve performance.

First of all, in nature, spinel represents a large family of minerals with a general formula of AB_2X_4, including spinel $MgAl_2O_4$ (which this mineral family and the structure are named after), gahnite $ZnAl_2O_4$, magnetite Fe_3O_4 (i.e. $Fe^{2+}(Fe^{3+})_2O_4$), cuprospinel $CuFe_2O_4$, chromite $FeCr_2O_4$ and many others.[90] The presence of such abundant minerals with versatile chemistry illustrates the phase stability of the spinel structure. This phase stability applies to battery-related transition metal oxides as well. For example, according to the phase diagram calculated by Materials Project,[91] spinel is the thermodynamically stable structure for both $LiNi_2O_4$ and $LiCo_2O_4$ compositions, which has been proved by *in situ* heating experiments.[92] Second, electrochemically, the stability of spinel is implied by the high voltages of TM redox couples in the spinel structure. For example, in spinel cathodes, Ni^{3+}/Ni^{2+} has a redox potential of about 4.6 V vs. Li^+/Li, Ni^{4+}/Ni^{3+} has a redox potential of about 4.8 V vs. Li^+/Li, Mn^{4+}/Mn^{3+} has a redox potential of about 4.0 V vs. Li^+/Li, and Mn^{5+}/Mn^{4+} has a redox potential well above 5.0 V vs. Li^+/Li.[93] These redox voltages are generally much higher than their respective values in layered cathodes, if we consider the average discharge voltage of about 3.8 V (vs. Li^+/Li) for Ni-rich cathodes (that mainly operates on Ni^{4+}/Ni^{3+}) as a reference.[94] (Note that the redox potentials are even higher in olivine-structure phosphates, with Ni^{3+}/Ni^{2+} of about 5 V, Ni^{4+}/Ni^{3+} of about 5.3 V and Mn^{4+}/Mn^{3+} of about 4.8 V vs. Li^+/Li, which is also a structure with high stability.[95]) Such high redox voltages could be understood by the site energy of Li^+. In spinel cathodes, Li^+ reside in tetrahedral sites that are corner-shared with neighboring TM-O octahedra, while in layered cathodes Li^+ reside in octahedral sites that are edge-shared with neighboring TM-O octahedra. With longer Li-TM distances, Li^+ in spinel cathodes experience less Coulombic repulsion from neighboring cations and are thus more energetically stable, compared to the case in layered cathodes. This raises the equilibrium voltage of TM redox because adding/removing electrons in LIB electrodes must also involve simultaneous insertion/removal of Li^+ to compensate charge. On the other hand, the high redox voltages

should not come from contribution by electronic energy. This is because strong hybridization between TM 3*d* orbitals and oxygen *2p* orbitals increases the energy of TM-O anti-bonding states (thus lowering TM cation-redox voltages) and lowers the energy of TM-O bonding states (thus increasing O anion-redox voltages). Atomistically, the hybridization could be stronger than the layered case considering the higher average TM valence of +3.5 in spinel cathodes than in layered cathodes, which results in stronger Coulombic attraction between TM and oxygen ions and creates shorter TM-O bonds. This strong hybridization is further supported by the inaccessible oxygen redox with a band edge at about 5.0 V (vs. Li^+/Li),[96] compared with the Li-O-Li configuration enabled oxygen redox at about 4.5 V vs. Li^+/Li in Li-rich layered cathodes.[97] As a result, anion redox is typically not observed in $LiMn_2O_4$ nor $LiNi_{0.5}Mn_{1.5}O_4$, even up to 5.0 V vs. Li^+/Li for the latter.

However, in Li-rich spinels such as $Li_4Mn_5O_{12}$ where Li substitute some of the Mn, TM-O hybridization becomes weaker, upshifting the O-orbital energy level and rendering anion redox accessible at a lower voltage. Liu *et al*.[31] recently reported hybrid anion- and cation-redox (HACR)[32] activities in a Li-rich spinel with nominal composition close to $Li_4Mn_5O_{12}$, where oxygen anion-redox (*m,a*-contribution) and TM cation-redox (*p,c*-contribution) reactions could give a theoretical capacity of 243.9 mAh/g (illustrated in **Figure 9**). Some oxygen loss in the initial formation cycles could reduce the average valence of Mn, and cause increasing proportion of cation-redox in later cycles, but reversible oxygen anion-redox are likely still present. Due to the low-temperature (400 °C) solid-state synthesis, the primary particle sizes are small, and smaller cathode particles seems to tolerate Mn^{3+} Jahn-Teller distortion better.

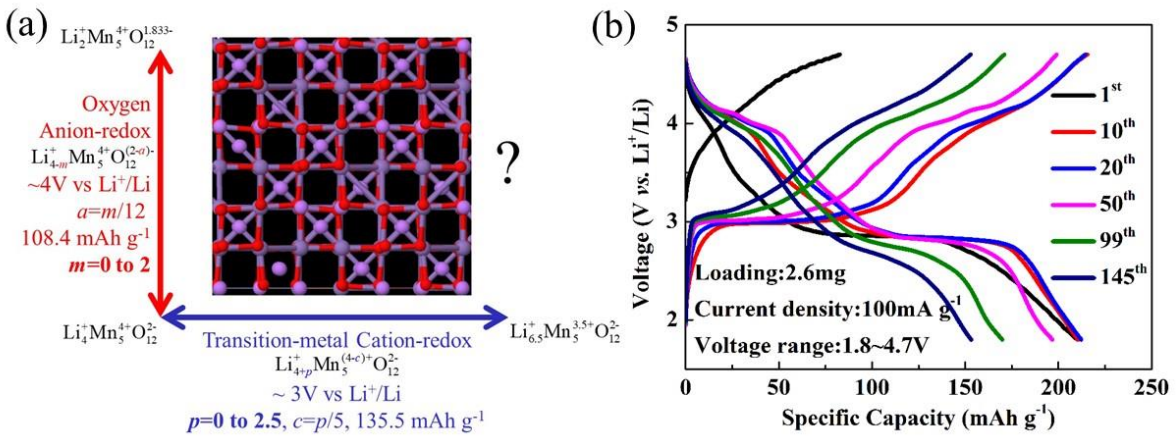

Figure 9. a) Hybrid oxygen anion-redox and TM cation-redox reaction coordinate as: $Li_2^+Mn_5^{4+}O_{12}^{1.833-} \leftrightarrow Li_4^+Mn_5^{4+}O_{12}^{2-} \leftrightarrow Li_{6.5}^+Mn_5^{3.5+}O_{12}^{2-}$. The inset shows spinel $Li(Mn_{5/3}Li_{1/3})O_4$ with long-range order of the 1/6 Li_{Mn} substitutions. b) Voltage profile of the $Li_4Mn_5O_{12}$-like half cells at the 20th cycle at a current density of 100 mA/g cycled between 1.8–4.7 V vs. Li^+/Li at room temperature. Reproduced with permission.[31] Copyright 2019, Royal Society of Chemistry.

Lastly, spinel cathodes are known for high thermal runaway temperature and good safety, which suggest good thermal stability. The aforementioned phase, structural, electrochemical and thermal stability of the "good spinel" $Li(TM)_2O_4$ structures as well as "bad spinel" structures like $(TM)_3O_4$ where all conduction channels are blocked, correlate with their frequent appearances on the surface of various layered cathodes, especially under high-voltage, high temperature and prolonged cycling. For example, the following observations were reported in $LiCoO_2$: using transmission electron microscopy (TEM) and electron diffraction, Wang *et al.*[98] observed cation occupancy at 8a tetrahedral sites and partial phase transformation to spinel-type ordering at the surface of $LiCoO_2$ cycled between 2.5 V and 4.35 V vs. Li^+/Li; Yazami *et al.*[99] observed the formation of cubic spinel phase under TEM in $LiCoO_2$ after aging at 4.7 V vs. Li^+/Li for 10 h as well as irreversible loss in capacity and rate

capabilities; using EELS, Kikkawa *et al.*[100] observed Co_3O_4-like phase and Li-inserted Co_3O_4 at the surface of $LiCoO_2$ charged to 40%, 60% and 100% capacity; using HAADF-STEM and EELS, Tan *et al.*[101] observed Co_3O_4-like phase at the surface of epitaxial $LiCoO_2$ electrode films after charged to 4.2 V vs. Li^+/Li; using HAADF-STEM, Yano *et al.*[102] observed spinel-like phase at the surface of $LiCoO_2$ cycled at 2.5 – 4.7 V vs. Li^+/Li; using high-resolution TEM, Seong *et al.*[103] reported the formation of disordered spinel $Li_2Co_2O_4$ phase and spinel Co_3O_4 nanoparticles at the surface of $LiCoO_2$ cycled at 3.0-4.6/4.8 V vs. Li^+/Li; and Yoon *et al.*[35b] observed spinel-like phase (**Figure 10**) at the surface of $LiCoO_2$ cycled at 3.0 – 4.45 V vs. Li^+/Li, while 5% Ni doping is effective in modifying the production of the surface phase transformation to a cation-mixed phase. Similar observations were also made in NCM/NCA with various Ni/Co/Mn/Al ratios. For example, Nam *et al.*[104] used *in situ* synchrotron X-ray diffraction/absorption technique and TEM to study the structural evolution of overcharged $LiNi_{1/3}Co_{1/3}Mn_{1/3}O_2$ and $LiNi_{0.8}Co_{0.15}Al_{0.05}O_2$, and showed by XRD (**Figure 11**) that $Li_{0.33}Ni_{1/3}Co_{1/3}Mn_{1/3}O_2$ transformed to a spinel phase at 337 ^oC, while $Li_{0.33}Ni_{0.8}Co_{0.15}Al_{0.05}O_2$ transformed to mixed phases of spinel and rocksalt at 256 ^oC before turning into pure rocksalt at 471 ^oC. Jung *et al.*[105] observed minor rocksalt phase and dominating spinel phase at the surface of $LiNi_{0.5}Co_{0.2}Mn_{0.3}O_2$ cycled at 3.0 – 4.5 V (vs. Li^+/Li), and spinel phase enclosed by rocksalt phase at the surface of $LiNi_{0.5}Co_{0.2}Mn_{0.3}O_2$ cycled at 3.0 – 4.8 V (vs. Li^+/Li), while $LiNi_{0.5}Co_{0.2}Mn_{0.3}O_2$ cycled at 3.0 – 4.3 V (vs. Li^+/Li) shows little phase transformation. Lin *et al.*[106] used atomic resolution annular dark-field STEM to investigate the surface reconstruction of $LiNi_{0.4}Mn_{0.4}Co_{0.18}Ti_{0.02}O_2$ and found a thin layer of spinel structure bridging the un-transformed layered structure (with Ni^{2+}, Mn^{4+} and Co^{3+}) and the transformed rocksalt structure (with Ni^{2+}, Mn^{2+} and Co^{2+}). Using HAADF-STEM and electron diffraction, Kim *et al.*[107] observed the formation of spinel structure around micro-cracks inside the primary particles of $LiNi_{0.6}Co_{0.2}Mn_{0.2}O_2$ cycled at 3.0 – 4.45 V (vs. Li^+/Li) at 60 ^oC.

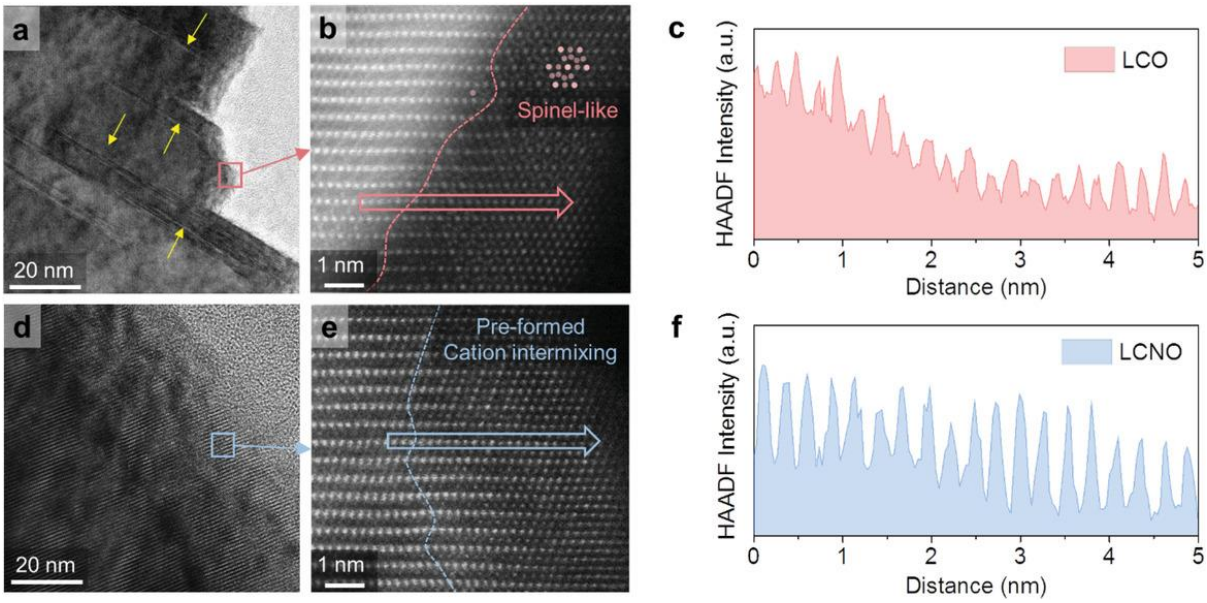

Figure 10. Surface structure of (a-b) $LiCoO_2$ and (d-e) $LiNi_{0.05}Co_{0.95}O_2$, and HAADF profile of (c) $LiCoO_2$ and (f) $LiNi_{0.05}Co_{0.95}O_2$, all cycled at 3.0 – 4.45 V vs. Li^+/Li. Spinel-like phase forms at the surface of cycled $LiCoO_2$, while cation-mixed phase forms at the surface of $LiNi_{0.05}Co_{0.95}O_2$. Reproduced with permission.[35b] Copyright 2020, John Wiley & Sons, Inc.

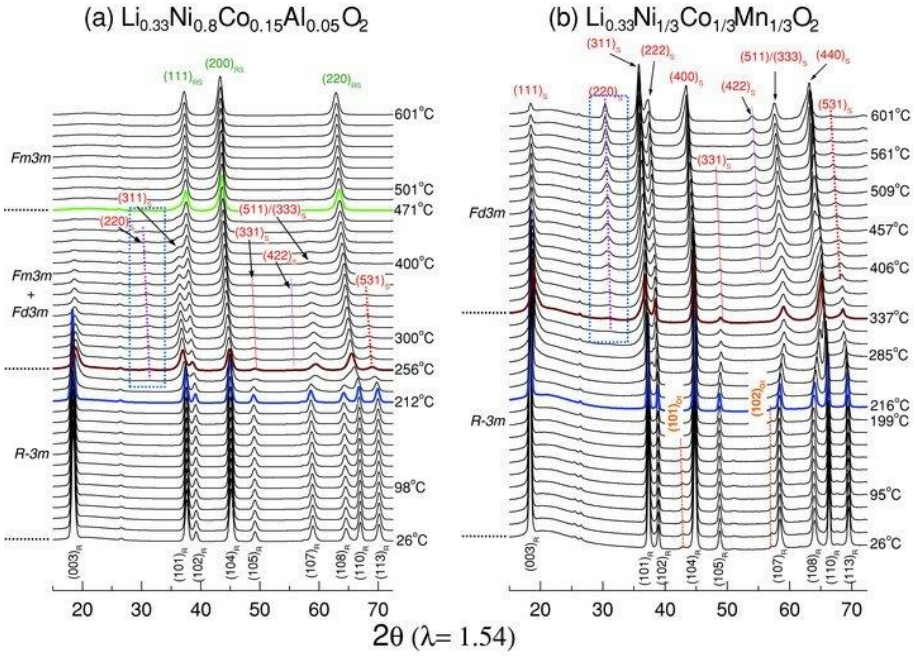

Figure 11. XRD patterns of a) $Li_{0.33}Ni_{0.8}Co_{0.15}Al_{0.05}O_2$ and b) $Li_{0.33}Ni_{1/3}Co_{1/3}Mn_{1/3}O_2$ to reveal the structural and phase evolutions during *in situ* heating up to 600 °C. Subscript R denotes rhombohedral layered structure ($R\bar{3}m$), S denotes spinel structure ($Fd\bar{3}m$), and RS denotes

rocksalt structure ($Fm\bar{3}m$). Reproduced with permission.[104] Copyright 2013, John Wiley & Sons, Inc.

Transformation to spinel is more pronounced in layered Li-rich cathodes that utilize both cation (TM) and anion (O) redox. For example, with combined XRD, high-resolution TEM and Raman spectroscopy, Hong *et al*.[108] confirmed the transformation to spinel-like domains in the layered framework of $Li_{1.2}Ni_{0.2}Mn_{0.6}O_2$ cycled at 2.0 – 4.8 V vs. Li^+/Li. Similarly, Ito *et al*.[109] observed by atomic resolution HAADF-STEM and selected-area electron diffraction (SEAD) the formation of the spinel structure in $Li_{1.2}Ni_{0.17}Co_{0.07}Mn_{0.56}O_2$ at 4.5 V plateau during the first charge to 4.8 V vs. Li^+/Li, Xu *et al*.[110] observed the formation of a defect-spinel phase at the surface of $Li_{1.2}Ni_{0.2}Mn_{0.6}O_2$ cycled at 2.0 – 4.8 V vs. Li^+/Li under high-resolution STEM, Gu *et al*.[111] observed the formation of $LiMn_2O_4$-like cubic spinel in $Li_{1.2}Ni_{0.2}Mn_{0.6}O_2$ and $Li_{1.2}Ni_{0.1}Co_{0.175}Mn_{0.525}O_2$ cycled at 2.0 – 4.6 V vs. Li^+/Li (after three formation cycles at 2.0 – 4.8V vs. Li^+/Li) under TEM, Zheng *et al*.[112] observed the formation of spinel-like phase at the surface of $Li_{1.2}Ni_{0.2}Mn_{0.6}O_2$ cycled at 2.0 – 4.8 V vs. Li^+/Li under STEM, and Yan *et al*.[113] observed the formation of $LiMn_2O_4$-type or M_3O_4-type (*M*: transition metal) spinel (**Figure 12**) in $Li_{1.2}Ni_{0.2}Mn_{0.6}O_2$ cycled at 2.0 – 4.7 V vs. Li^+/Li under STEM. Interestingly, Yan *et al*.[114] observed the formation of spinel-like structure as well as a large population of nano-voids not only at the surface but also in the bulk of $Li_{1.2}Ni_{0.2}Mn_{0.6}O_2$ cycled at 2.0 – 4.8 V vs. Li^+/Li by STEM-HAADF. Therefore, it is clear that spinel structure also serves as a degradation product of layered Li-rich cathodes.

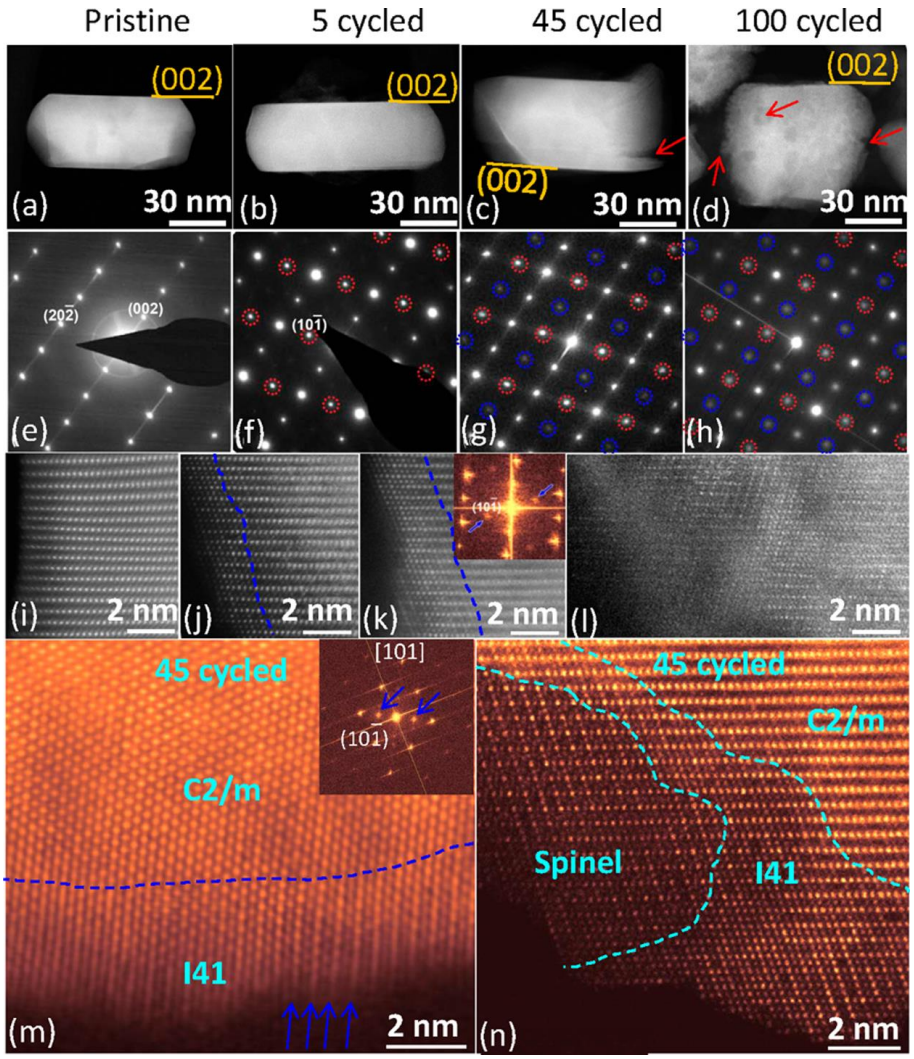

Figure 12. (a-d) Low-magnification STEM-HAADF images and (e-h) SAED pattern along the [010] zone axis of $Li_{1.2}Ni_{0.2}Mn_{0.6}O_2$ cycled under various conditions. (i-l) High-resolution STEM-HAADF images for the surfaces of cycled particles. (m, n) [010] zone axis STEM-HAADF images identified spinel structure and I41 structure in 45 cycled samples. Reproduced with permission.[113] Copyright 2014, American Chemical Society.

The above observations in layered $LiCoO_2$, NCM, NCA, and Li-rich cathodes raise an interesting question: what is the atomistic process and the driving force for the transformation of layered structures to spinel-like structures (either good or bad) upon electrochemical cycling? There could be several possible reasons. First of all, considering the structural relationship between layered and spinel structures shown in **Figure 2** and **Figure 13**[115], TM ion migration

from TM layer to Li layer is clearly involved, which could be both thermodynamically and kinetically more favorable at highly charged (i.e. delithiated) states than at discharged (i.e. stoichiometric) states. Second, the "layeredness" (i.e. cation ordering with alternating (111) planes of TM layers and Li layers) is driven by the difference in the charge and size between TM ions and Li^+. For example, Co being +3 valence and much smaller than Li^+ promotes planar Li-TM-Li-TM concentration wave in $LiCoO_2$, maintained even at high temperatures of > 1000 ^oC in air; in comparison, Ni being only +2 valence and similar in size with Li^+ tends to cation-mix with Li^+, which sets strict requirements on the synthesis conditions (temperature and atmosphere) of $LiNiO_2$ and Ni-rich NCM/NCA. Therefore, since TM ions typically become more reduced at the surface of cycled cathodes due to anion-redox induced oxygen mobility and oxygen loss[32], the layeredness is difficult to maintain, which justifies why TM ions migrate into the Li layer (almost empty in highly charged states). Third, electrostatic repulsion between TM ions would tend to separate them apart, maximizing their distances and offering a driving force for cation ordering into a spinel-like pattern. (Remember in the spinel structure, B-site cations only occupy half of the octahedral sites in an edge-sharing manner.) Lastly, some reduced cations such as Co^{2+} and Mn^{3+} may prefer tetrahedral sites (Co^{2+}: $e_g^4 t_{2g}^3$, Mn^{3+}: $e_g^4 t_{2g}^0$), which also promotes the formation of the "bad spinel" structures (there is no cation tetrahedral occupancy in layered structure). Nevertheless, in addition to the above general considerations, the detailed mechanism and kinetics of the phase transformation could vary with different materials and testing conditions (such as voltage, time, temperature, and the type of electrolytes), which is worthwhile for future investigations.

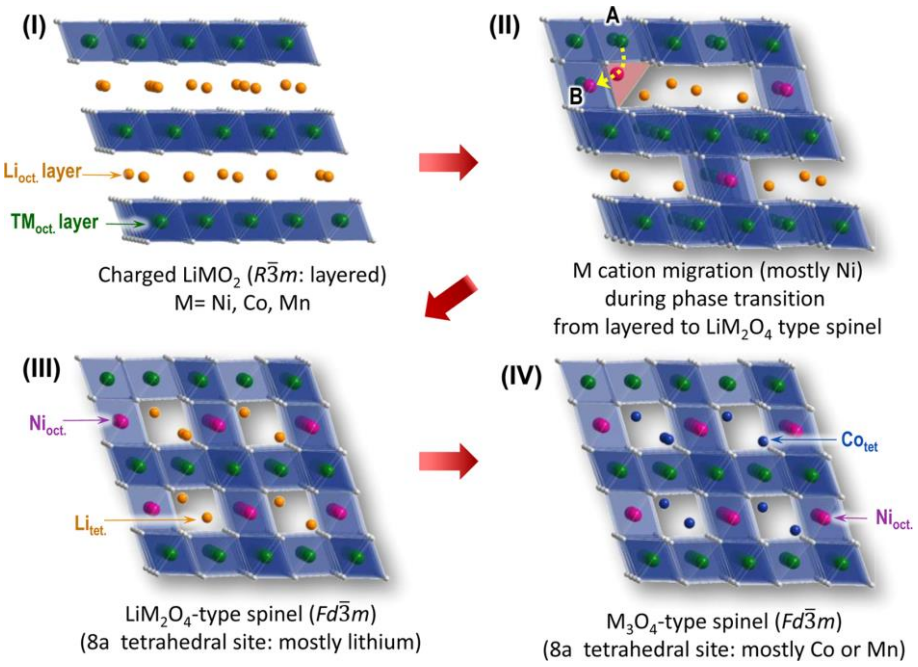

Figure 13. Schematics illustrating cation migration and structure reconstruction from (I) perfect layered structure, to (II) partially cation-mixed layered structure, to (III) $LiMn_2O_4$-type "good" spinel structure and to (IV) M_3O_4-type "bad" spinel structure. M denotes transition metal elements. The process was originally summarized for structural evolution during heat treatment, but it could be also applicable for evolution during electrochemical cycling. Reproduced with permission.[115] Copyright 2014, American Chemical Society.

On the other hand, the robustness of the spinel structure inspires people to integrate it with other structures to improve structural stability. One such effort is to integrate the "good spinel" structure with a layered one to prepare a "composite" electrode, such as xLiNi$_{0.5}$Mn$_{1.5}$O$_4$•(1−x)[Li$_2$MnO$_3$•LiNi$_{0.5}$Mn$_{0.5}$O$_2$] and xLi$_2$MnO$_3$•(1−x)Li$_{1+\delta}$Mn$_{2-\delta}$O$_4$ ($0 \leq \delta \leq 1/3$).[13c, 116] Another commonly practiced method is to coat a stable spinel structure over high energy density cathodes such as LiCoO$_2$, high-Ni NCM/NCA and Li-/Mn-rich materials. For example, spinel Li(Ni$_{0.31}$Co$_{0.11}$Mn$_{0.58}$)$_2$O$_4$ coated Li(Ni$_{0.54}$Co$_{0.12}$Mn$_{0.34}$)O$_2$, spinel LiMn$_2$O$_4$ coated Li$_{1.2}$Mn$_{0.6}$Ni$_{0.2}$O$_2$, spinel Li$_x$Co$_2$O$_4$ coated LiCoO$_2$, spinel LiMn$_{1.9}$Al$_{0.1}$O$_4$ coated Li(Ni$_{0.7}$Co$_{0.15}$Mn$_{0.15}$)O$_2$, and spinel Li$_{4/3}$Mn$_{5/3}$O$_4$ coated Li$_{1.214}$Mn$_{0.53}$Co$_{0.128}$Ni$_{0.128}$O$_2$ have been

reported in the literature[117], which demonstrate superior cycling stability over the uncoated materials. Herein, special attention should be paid to Mn^{4+}-based spinel including the well-known compositions of $Li_{4/3}Mn_{5/3}O_4$ and $LiNi_{0.5}Mn_{1.5}O_4$ as well as hypothetical ones of $xLi_{4/3}Mn_{5/3}O_4$•$(1-x)LiNi_{0.5}Mn_{1.5}O_4$ and $xLi_{4/3}Mn_{5/3}O_4$•$(1-x)LiAlMnO_4$, because they will not suffer from the damaging disproportionation reaction and Mn^{4+} is relatively catalytically-inactive compared to other widely used TM ions (e.g. $Co^{3+/4+}$ and $Ni^{3+/4+}$) in LIB cathodes. Zhang *et al.*[117e] successfully coated a uniform layer of $Li_4Mn_5O_{12}$ on Li-rich $Li_{1.2}Mn_{0.54}Co_{0.13}Ni_{0.13}O_2$, from which they obtained better capacity and voltage retention, reduced oxygen evolution, and mitigated "bad spinel"-like phase transformation. Zhu *et al.*[17] coated ~10 mm $LiCoO_2$ single-crystals with a lattice-coherent $LiMn_{0.75}Ni_{0.25}O_2$ surface layer (**Figure 14a**), which normally is not stable as a bulk layered phase, but is stabilized here as an epitaxial nanolayer to the $LiCoO_2$ single crystal. This layered $LiMn_{0.75}Ni_{0.25}O_2$ further transforms into a "good" (i.e., with percolating Li^+ diffusion channels) $LiMn_{1.5}Ni_{0.5}O_4$ spinel shell during the initial electrochemical cycles that completely wetted and wrapped the $LiCoO_2$ bulk (**Figure 14b**). The robust "good spinel" shell effectively prevented O_2 escape and Co dissolution, which drastically improved the cyclability of $LiCoO_2$ under high voltage cycling (3.0 – 4.6 V). Such novel spinel coatings are worthwhile to be further explored, probably assisted by innovative synthesis methods[32] that lead to more uniform conformal coating with better bonding to the host material.

Generally, if surface phase reconstruction has to happen, it is important to promote surface reconstruction to the "good spinel" phase $Li(TM)_2O_4$ instead of "bad spinel" surface phases like $(TM)_3O_4$. The defining characteristics of the "bad spinel" surface phase is the higher TM:O ratio (likely due to previous oxygen escape when charged to high voltages) and lower average valence of TM (lower than 3+). Such "bad spinel" (a) is more soluble in the liquid electrolyte than "good spinel", and (b) has TM packed in the tetrahedral sites in addition to the octahedral

sites due to crowding, thus blocking Li^+ diffusion paths. As a rule of thumb, "bad spinel" has TM:O ratio greater than 0.5 (as in the case of Co_3O_4 and Mn_3O_4), whereas the "good spinel" has TM:O ratio equal to or less than 0.5. In the **Figure 14** example, the Mn:Ni:O ratio of 3:1:8 managed to stay unchanged before and after electrochemical lithiation, and the coating stayed conformal due to pre-positioning of the Mn:Ni:O elements in the correct ratio to reconstruct into arguably the best spinel possible $LiMn_{1.5}Ni_{0.5}O_4$, with very little oxygen loss.

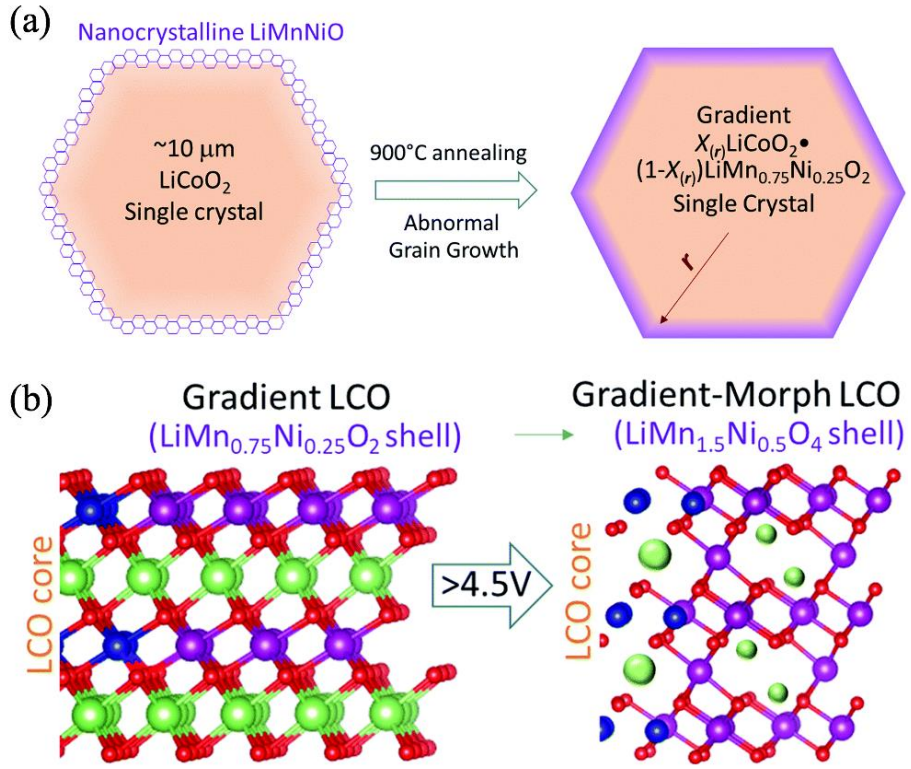

Figure 14. a) Schematic of gradient $LiCoO_2$ – $LiMn_{0.75}Ni_{0.25}O_2$ single crystal created by high temperature annealing. b) Formation of semi-coherent $LiMn_{1.5}Ni_{0.5}O_4$ shell on $LiCoO_2$ during initial electrochemical cycling, as the Mn:Ni:O ratio of 3:1:8 stay unchanged upon delithiation. Reproduced with permission.[17] Copyright 2020, Royal Society of Chemistry.

6. Spinel framework for high-rate and high-power-density batteries

"Good" cubic spinels $Li(TM)_2O_4$ are known for their 3D interconnected diffusion channels, which offer isotropic pathways for fast Li^+ intercalation and enable applications in high-rate

and high-power-density batteries. For spinel cathodes, both $LiMn_2O_4$ and $LiNi_{0.5}Mn_{1.5}O_4$ follow the solid-solution behavior during electrochemical cycling and their charge/discharge kinetics are controlled by Li^+ bulk diffusion. From an atomistic point of view, Li^+ diffusion takes place by a Li vacancy-mediated hopping mechanism between two neighboring 8a tetrahedral sites, through an unoccupied 16c octahedral site that face-shares with the two tetrahedra.[118] The Li^+ diffusivity of $LiMn_2O_4$ and $LiNi_{0.5}Mn_{1.5}O_4$ is experimentally measured to be in the range of 10^{-12} – 10^{-9} cm^2/s, by various techniques including galvanostatic intermittent titration technique (GITT), potentiostatic intermittent titration technique (PITT), electrochemical impedance spectroscopy (EIS), electrochemical voltage spectroscopy (EVS), and current pulse relaxation (CPR).[119] According to the random-walk diffusion model $(\text{diffusion distance})^2 = 6 \times (\text{diffusivity}) \times (\text{time})$, such a diffusivity would ensure 1 μm particles to be charged/discharged within 3 – 100s, which indicates good rate capability, and allows the usage of micron-sized particles to be used in high-rate applications with high (volumetric) energy/power density.[120] Nanomaterials with shorter diffusion distance could enable even better kinetics at the cost of packing density and stability, and well-designed hierarchical structures could benefit from both nano and micron length scales. For example, Lee *et al*.[121] synthesized agglomerated composite cathodes with nanosized Li-/Al-doped $LiMn_2O_4$ and well-dispersed carbon black in the secondary particle (**Figure 15**), which have superior high-rate performance of 101 mAh/g under 300 C at 24 °C, and 75 mAh/g under 100 C at −10 °C. Nevertheless, the practical application of spinel cathodes in high-rate LIBs is hindered by high-temperature degradation problems, which become worse under dynamic large-current-density operations. Therefore, further improvement in cycling stability is necessary to maximize the intrinsic advantages of spinel cathodes in high-rate applications, which often requires prolonged cycle life.

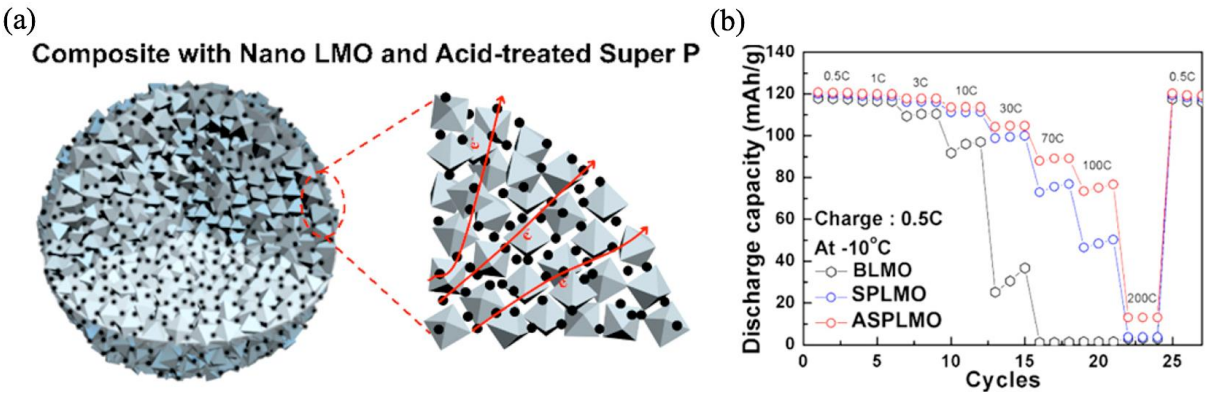

Figure 15. a) Cross section of nano-sized $Li_{1.015}Al_{0.06}Mn_{1.925}O_4$ (LMO) and acid-treated Super P composite (left), and electron percolation path (right). b) Discharge rate performance of electrodes at −10 °C (half cells, 3.0 – 4.5 V, BLMO: Ball-milled LMO, SPLMO: nano-LMO and Super P composite, ASPLMO: nano-LMO and acid-treated Super P composite). Reproduced with permission.[121] Copyright 2017, American Chemical Society.

Another example on the anode side is spinel $Li_4Ti_5O_{12}$, which has been commercialized as high-rate anodes in LIBs.[51, 122] In electrochemical cycling, Li^+ is inserted in $Li_4Ti_5O_{12}$ to trigger a spinel-to-rocksalt conversion reaction, which is charge-compensated by Ti^{4+}/Ti^{3+} redox and offers a voltage plateau at around 1.5 V (vs. Li^+/Li). Even though such a conversion reaction has sluggish kinetics in micron-sized $Li_4Ti_5O_{12}$, it turns out to be extremely fast in nano-$Li_4Ti_5O_{12}$.[123] Recently, through real-time characterizations of Li^+ diffusion kinetics by *in situ* electron energy loss spectroscopy and DFT calculations, Zhang *et al*.[124] rationalized the facile kinetics by polyhedral distortion and high-energy metastable intermediates (well above the ground state) at the two-phase boundaries, which is not accessible by the two end members of $Li_4Ti_5O_{12}$ and $Li_7Ti_5O_{12}$ (the lithiation product). This interface mediated diffusion kinetics were also observed by Wang *et al*.[123] in multi-phase lithium titanate hydrates (**Figure 16**), which were able to stably deliver 130 mAh/g at ~35 C over 10,000 cycles. The

characteristic of fast kinetics together with superior cycling stability and safety offered by the robust spinel framework makes $Li_4Ti_5O_{12}$ one of the best high-rate anodes in LIBs.

The above spinel candidates as high-rate LIB cathodes/anodes make it worthwhile to think about the mechanistic reason and effective utilization of the beneficial spinel framework for Li^+ diffusion, which was laid out by a thoughtful analysis given by Urban *et al*.[125] Generally speaking, the macroscopic Li^+ bulk diffusion in battery electrodes is enabled by a globally continuous or percolating diffusion pathway, and locally, it is rate-limited by the available hopping path with the lowest energy barrier. On one hand, the "good spinel" structure has no problem in terms of global diffusion, because of the 3D connected diffusion channel schematically plotted in **Figure 2b**. Locally, Urban *et al*. offered a model to correlate the Li^+ diffusion barrier with the number of neighboring octahedral TM ions for the saddle-point tetrahedral Li^+ in rocksalt-based structure (recall that layered structure can be viewed as a cation-ordered rocksalt structure). This model is based on the critical role of Coulombic repulsion between Li^+ and TM ions, which peaks when the Li^+ is at the saddle point of the migration pathway (i.e. tetrahedral site in the rocksalt structure) due to very short Li-TM distance. Note that the distance between neighboring face-sharing octahedral and tetrahedral sites is much shorter than the distance between neighboring edge-sharing octahedral and octahedral sites. Therefore, Li^+ with the least (i.e. zero) neighboring TM ions should have the smallest migration barrier, and a percolating network by so-called 0-TM Li^+ is responsible for the long-range diffusion in Li-rich disordered rocksalt cathodes.[16g] This model can be generalized to the spinel structure, where the saddle-point octahedral Li^+ is only in contact with empty face-sharing tetrahedral sites. In this sense, Li^+ migration in the spinel structure always takes place by 0-TM mode, which rationalizes the origin of its fast diffusion kinetics. In the spinel-like low-temperature $LiCoO_2$ structure (similar structure to the lithiated spinel or tetragonal rocksalt $Li_2Mn_2O_4$, where Co ordering in the cation sublattice is the same as the Mn

pattern in $LiMn_2O_4$), 0-TM mode is also available, which could help enhance diffusion kinetics. Such local structure with partial spinel-like order has been recently demonstrated by Ji *et al.*[15b] in Li-rich oxyfluorides with compositions of $Li_{1.68}Mn_{1.6}O_{3.7}F_{0.3}$ and $Li_{1.68}Mn_{1.6}O_{3.4}F_{0.6}$. The oxyfluorides are cycled on combined cationic and anionic redox and show excellent electrochemical performance with high capacity of > 360 mAh/g, high energy density of > 1100 Wh/kg and ultrafast rate capability up to 2000 mA/g (> 120 C) when cycled between 1.5 V and 4.8 V (vs. Li^+/Li). This highlights the great promise of utilizing spinel and spinel-like structures to design novel high-rate cathode materials, as well as engineered cationic and anionic redox activities.[126]

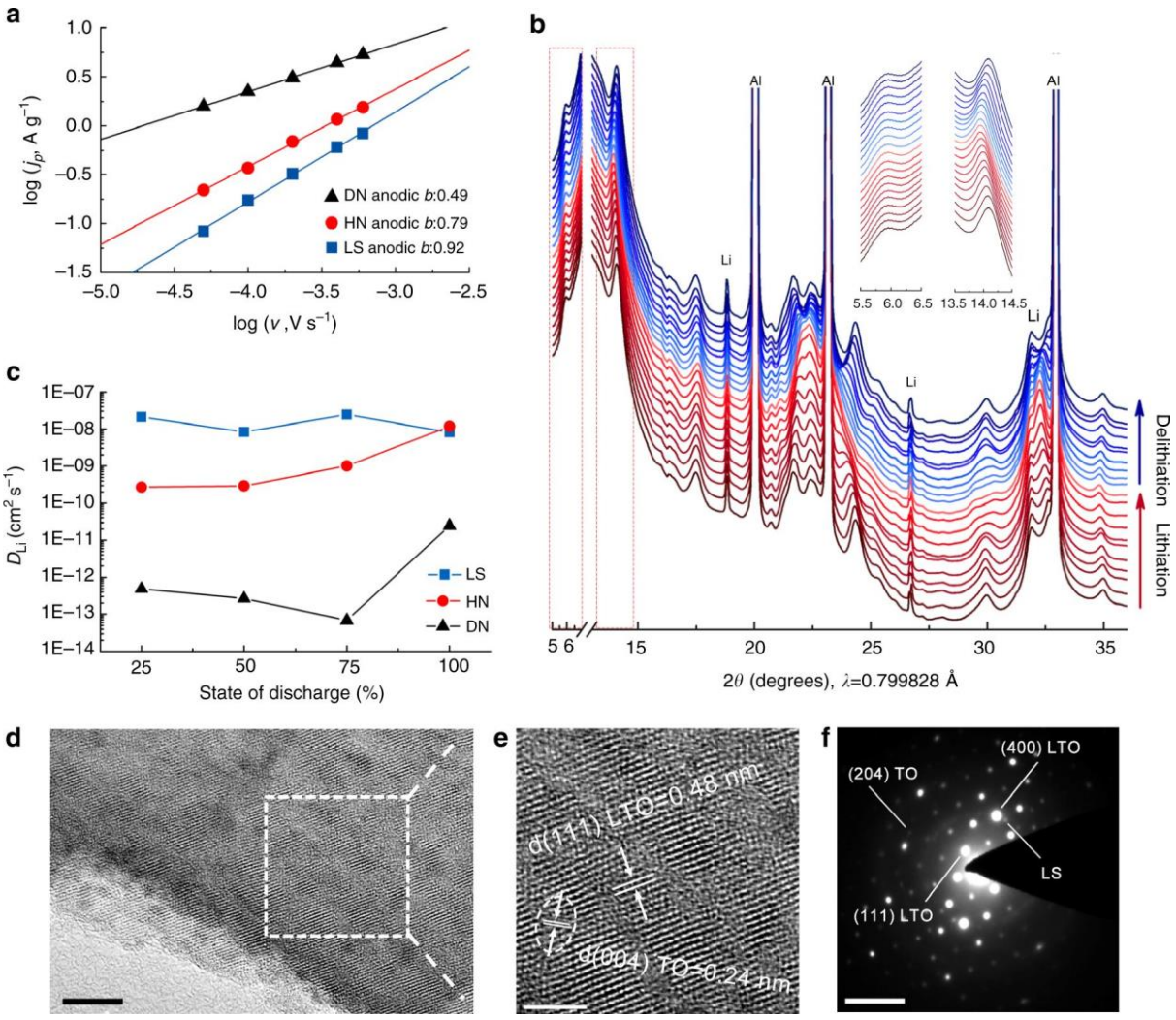

Figure 16. a) *b*-value analysis and c) calculated Li^+ diffusivity of three multi-phase lithium titanate hydrate composites: a hydrated nanocomposite (HN), a low-temperature treated layered-structure nanocomposite (LS) and a high-temperature treated dried nanocomposite (DN). b) *In situ* synchrotron XRD of LS electrode cycled at 100 mA/g. d) HRTEM image and f) SAED pattern of HN sample. e) Magnified regime of (d) showing $Li_4Ti_5O_{12}$-like and TiO_2-like phases. Reproduced with permission.[123] Copyright 2017, Springer Nature.

7. Conclusion and remarks

To summarize, the fundamental understanding of spinel $LiMn_2O_4$ cathode and its derivative were reviewed in this article, which provides valuable insights for the future development of LIB cathodes. With advantages especially in low cost, good thermal stability, high rate capability and ease of synthesis, the optimized spinel cathodes such as $LiMn_2O_4$ and $LiNi_{0.5}Mn_{1.5}O_4$ are promising in future applications of energy storage systems, power tools and electric vehicles.

We believe the following aspects are of central importance in spinel and related cathodes:

(1) More fundamental studies should be conducted to better understand the degradation mechanisms of spinel cathodes, especially the main problems of TM dissolution and surface/interface instability. Such knowledge should be transferable to other electrode materials, especially Mn-containing ones.

(2) Further development of spinel cathodes relies on optimizations on bulk doping, control of dopant distribution, coating, liquid electrolytes and potential applications in all-solid-state batteries. Special attention to surface doping and development of new liquid electrolytes are recommended. Machine learning and robotic synthesis could potentially be helpful in optimizations in the hyper-space of compositions and various processing parameters.

(3) Spinel structures can be integrated in the bulk and/or at the surface of other high-capacity

cathode materials, especially the layered cathodes that share the same oxygen sublattice. Special attention should be paid to the elements and valence of the spinel stabilizer, whereas catalytically-active TM ions should be avoided. More fundamental studies are suggested to understand the phase evolution and transformation dynamics at the surface of high-capacity cathodes, preferentially under dynamic conditions, to guide the reconstruction toward "good spinel" surface phases with percolating Li conduction pathways, instead of "bad spinel" surface phases where such pathways are blocked by TMs. As a rule of thumb, "bad spinel" has TM:O ratio greater than 0.5 (as in the case of Co_3O_4 and Mn_3O_4), likely due to oxygen loss in electrochemical cycling, whereas the "good spinel" has TM:O ratio equal to or less than 0.5. For instance, $LiMn_2O_4$ spinel is obviously a "good spinel", but with cycling this spinel is naturally subjected to a certain degree of surface oxygen loss, which in turn leads to the gradual formation of the "bad" Mn_3O_4 spinel. "Bad spinels" are bad because they are more soluble in the liquid electrolyte due to lower TM valence (less than 3+), and they also block Li diffusion paths and greatly increase the impedance, with TMs sitting at tetrahedral sites in addition to octahedral sites due to crowding. If the cathode surface has to reconstruct, being able to distinguish the "good spinel" from the "bad spinel" surface phases, and guiding the reconstruction toward a "good spinel", would be key.

(4) Spinel structures and rocksalt structures with spinel-like order could be beneficially used to design new cathode materials for high-energy density applications. To simultaneously increase the capacity, Li-excess compositions should be explored with activated anion redox. The fundamental mechanisms of fast kinetics and reversible hybrid anion- and cation-redox mechanisms in the spinel structure are worthwhile for detailed investigations in the future.

Acknowledgment

We acknowledge support by the Department of Energy, Basic Energy Sciences, under award number DE-SC0002633 (Chemomechanics of Far-From-Equilibrium Interfaces), and the U.S. Department of Energy (USDOE), Office of Energy Efficiency and Renewable Energy (EERE), Advanced Manufacturing Office (AMO) R&D Projects Emerging Research Exploration, under DOE Idaho Operations Office with contract no. DE-AC07-05ID14517.

Conflict of interest

The authors declare no conflict of interest.

References

[1] NobelPrize.org, The Nobel Prize in Chemistry 2019, https://www.ncbi.nlm.nih.gov/pubmed/28931813, accessed: Feb 15, 2020.

[2] K. Mizushima, P. C. Jones, P. J. Wiseman, J. B. Goodenough, *Mater Res Bull* **1980**, 15, 783.

[3] a) M. M. Thackeray, W. I. F. David, P. G. Bruce, J. B. Goodenough, *Mater Res Bull* **1983**, 18, 461; b) M. M. Thackeray, P. J. Johnson, L. A. Depicciotto, P. G. Bruce, J. B. Goodenough, *Mater Res Bull* **1984**, 19, 179.

[4] A. K. Padhi, K. S. Nanjundaswamy, J. B. Goodenough, *Journal of the Electrochemical Society* **1997**, 144, 1188.

[5] J. B. Goodenough, *Journal of Power Sources* **2007**, 174, 996.

[6] J. C. Hunter, *J Solid State Chem* **1981**, 39, 142.

[7] M. M. Thackeray, W. I. F. David, J. B. Goodenough, *Mater Res Bull* **1982**, 17, 785.

[8] a) Y. Y. Xia, M. Yoshio, *Journal of the Electrochemical Society* **1996**, 143, 825; b) G. Pistoia, D. Zane, Y. Zhang, *Journal of the Electrochemical Society* **1995**, 142, 2551; c) J. Sugiyama, T. Atsumi, T. Hioki, S. Noda, N. Kamegashira, *J Alloy Compd* **1996**, 235, 163; d) J. M. Tarascon, W. R. Mckinnon, F. Coowar, T. N. Bowmer, G. Amatucci, D. Guyomard, *Journal of the Electrochemical Society* **1994**, 141, 1421; e) D. Guyomard, J. M. Tarascon, *Solid State Ionics* **1994**, 69, 222; f) G. G. Amatucci, A. Blyr, C. Sigala, P. Alfonse, J. M. Tarascon, *Solid State Ionics* **1997**, 104, 13; g) A. Du Pasquier, A. Blyr, P. Courjal, D. Larcher, G. Amatucci, B. Gerand, J. M. Tarascon, *Journal of the Electrochemical Society* **1999**, 146, 428; h) G. Amatucci, A. Du Pasquier, A. Blyr, T. Zheng, J. M. Tarascon, *Electrochim Acta* **1999**, 45, 255; i) J. Cho, M. M. Thackeray, *Journal of the Electrochemical Society* **1999**, 146, 3577.

[9] a) M. M. Thackeray, A. Dekock, M. H. Rossouw, D. Liles, R. Bittihn, D. Hoge, *Journal of the Electrochemical Society* **1992**, 139, 363; b) M. M. Thackeray, *Prog Solid State Ch* **1997**, 25, 1.

[10] R. J. Gummow, A. Dekock, M. M. Thackeray, *Solid State Ionics* **1994**, 69, 59.

[11] a) Q. M. Zhong, A. Bonakdarpour, M. J. Zhang, Y. Gao, J. R. Dahn, *Journal of the Electrochemical Society* **1997**, 144, 205; b) K. Amine, H. Tukamoto, H. Yasuda, Y. Fujita, *Journal of Power Sources* **1997**, 68, 604; c) A. Manthiram, K. Chemelewski, E. S. Lee, *Energ Environ Sci* **2014**, 7, 1339.

[12] a) M. H. Rossouw, D. C. Liles, M. M. Thackeray, *J Solid State Chem* **1993**, 104, 464; b) P. Kalyani, S. Chitra, T. Mohan, S. Gopukumar, *Journal of Power Sources* **1999**, 80, 103; c) A. Manthiram, J. C. Knight, S. T. Myung, S. M. Oh, Y. K. Sun, *Adv Energy Mater* **2016**, 6, 1501010; d) J. M. Zheng, S. J. Myeong, W. R. Cho, P. F. Yan, J. Xiao, C. M. Wang, J. Cho, J. G. Zhang, *Adv Energy Mater* **2017**, 7, 1601284.

[13] a) A. R. Armstrong, P. G. Bruce, *Nature* **1996**, 381, 499; b) C. S. Johnson, N. Li, J. T. Vaughey, S. A. Hackney, M. M. Thackeray, *Electrochem Commun* **2005**, 7, 528; c) M. M. Thackeray, C. S. Johnson, J. T. Vaughey, N. Li, S. A. Hackney, *J Mater Chem* **2005**, 15, 2257.

[14] R. Schmuch, R. Wagner, G. Horpel, T. Placke, M. Winter, *Nature Energy* **2018**, 3, 267.

[15] a) J. M. Tarascon, E. Wang, F. K. Shokoohi, W. R. Mckinnon, S. Colson, *Journal of the Electrochemical Society* **1991**, 138, 2859; b) H. Ji, J. Wu, Z. Cai, J. Liu, D.-H. Kwon, H. Kim, A. Urban, J. K. Papp, E. Foley, Y. Tian, M. Balasubramanian, H. Kim, R. J. Clément, B. D. McCloskey, W. Yang, G. Ceder, *Nature Energy* **2020**, DOI: 10.1038/s41560-020-0573-1.

[16] a) J. R. Dahn, U. Vonsacken, C. A. Michal, *Solid State Ionics* **1990**, 44, 87; b) E. Rossen, C. D. W. Jones, J. R. Dahn, *Solid State Ionics* **1992**, 57, 311; c) E. Zhecheva, R. Stoyanova, *Solid State Ionics* **1993**, 66, 143; d) M. Yoshio, H. Noguchi, J. Itoh, M. Okada, T. Mouri, *Journal of Power Sources* **2000**, 90, 176; e) J. S. Weaving, F. Coowar, D. A. Teagle, J. Cullen, V. Dass, P. Bindin, R. Green, W. J. Macklin, *Journal of Power Sources* **2001**, 97-8, 733; f) Z. H. Lu, D. D. MacNeil, J. R. Dahn, *Electrochem Solid St* **2001**, 4, A191; g) J. Lee, A. Urban, X. Li, D. Su, G. Hautier, G. Ceder, *Science* **2014**, 343, 519.

[17] Z. Zhu, D. Yu, Z. Shi, R. Gao, X. Xiao, I. Waluyo, M. Ge, Y. Dong, W. Xue, G. Xu, W.-K. Lee, A. Hunt, J. Li, *Energ Environ Sci* **2020**, DOI: 10.1039/d0ee00231c.

[18] M. J. Lee, S. Lee, P. Oh, Y. Kim, J. Cho, *Nano Lett* **2014**, 14, 993.

[19] T. F. Yi, J. Mei, Y. R. Zhu, *Journal of Power Sources* **2016**, 316, 85.

[20] N. Xu, H. B. Zhou, Y. H. Liao, G. J. Li, M. Q. Xu, W. S. Li, *Solid State Ionics* **2019**, 341, 115049.

[21] a) P. He, H. R. Wang, L. Qi, T. Osaka, *Journal of Power Sources* **2006**, 160, 627; b) H. J. Noh, S. Youn, C. S. Yoon, Y. K. Sun, *Journal of Power Sources* **2013**, 233, 121.

[22] L. W. Liang, G. R. Hu, F. Jiang, Y. B. Cao, *J Alloy Compd* **2016**, 657, 570.

[23] N. T. Wu, H. Wu, W. Yuan, S. J. Liu, J. Y. Liao, Y. Zhang, *J Mater Chem A* **2015**, 3, 13648.

[24] a) F. He, X. Q. Wang, C. Q. Du, A. P. Baker, J. W. Wu, X. H. Zhang, *Electrochim Acta* **2015**, 153, 484; b) B. Qiu, J. Wang, Y. G. Xia, Y. Z. Liu, L. F. Qin, X. Y. Yao, Z. P. Liu, *Journal of Power Sources* **2013**, 240, 530; c) L. Ku, Y. X. Cai, Y. T. Ma, H. F. Zheng, P. F. Liu, Z. S. Qiao, Q. S. Xie, L. S. Wang, D. L. Peng, *Chem Eng J* **2019**, 370, 499.

[25] W. J. Zhang, *Journal of Power Sources* **2011**, 196, 2962.

[26] S. K. Martha, J. Grinblat, O. Haik, E. Zinigrad, T. Drezen, J. H. Miners, I. Exnar, A. Kay, B. Markovsky, D. Aurbach, *Angew Chem Int Edit* **2009**, 48, 8559.

[27] J. B. Goodenough, K. S. Park, *J Am Chem Soc* **2013**, 135, 1167.

[28] R. A. House, P. G. Bruce, *Nature Energy* **2020**, 5, 191.

[29] M. D. Radin, S. Hy, M. Sina, C. C. Fang, H. D. Liu, J. Vinckeviciute, M. H. Zhang, M. S. Whittingham, Y. S. Meng, A. Van der Ven, *Adv Energy Mater* **2017**, 7, 1602888.

[30] a) M. M. Thackeray, J. R. Croy, E. Lee, A. Gutierrez, M. N. He, J. S. Park, B. T. Yonemoto, B. R.

Long, J. D. Blauwkamp, C. S. Johnson, Y. Shin, W. I. F. David, *Sustain Energ Fuels* **2018**, 2, 1375; b) C. Masquelier, M. Tabuchi, K. Ado, R. Kanno, Y. Kobayashi, Y. Maki, O. Nakamura, J. B. Goodenough, *J Solid State Chem* **1996**, 123, 255; c) J. M. Paulsen, J. R. Dahn, *Chem Mater* **1999**, 11, 3065.

[31] Y. Liu, G. Liu, H. Xu, Y. H. Zheng, Y. H. Huang, S. Li, J. Li, *Chem Commun* **2019**, 55, 8118.

[32] Z. Zhu, D. W. Yu, Y. Yang, C. Su, Y. M. Huang, Y. H. Dong, I. Waluyo, B. M. Wang, A. Hunt, X. H. Yao, J. Lee, W. J. Xue, J. Li, *Nature Energy* **2019**, 4, 1049.

[33] R. J. Gummow, D. C. Liles, M. M. Thackeray, *Mater Res Bull* **1993**, 28, 1249.

[34] a) E. Peled, *Journal of the Electrochemical Society* **1979**, 126, 2047; b) M. Winter, B. Barnett, K. Xu, *Chemical Reviews* **2018**, 118, 11433.

[35] a) R. Robert, C. Bunzli, E. J. Berg, P. Novak, *Chem Mater* **2015**, 27, 526; b) M. Yoon, Y. Dong, Y. Yoo, S. Myeong, J. Hwang, J. Kim, S. H. Choi, J. Sung, S. J. Kang, J. Li, J. Cho, *Adv Funct Mater* **2020**, 30, 1907903; c) K. Luo, M. R. Roberts, R. Hao, N. Guerrini, D. M. Pickup, Y. S. Liu, K. Edstrom, J. H. Guo, A. V. Chadwick, L. C. Duda, P. G. Bruce, *Nat Chem* **2016**, 8, 684.

[36] a) C. Zhan, T. P. Wu, J. Lu, K. Amine, *Energ Environ Sci* **2018**, 11, 243; b) A. Bhandari, J. Bhattacharya, *Journal of the Electrochemical Society* **2017**, 164, A106.

[37] a) A. Blyr, C. Sigala, G. Amatucci, D. Guyomard, Y. Chabre, J. M. Tarascon, *Journal of the Electrochemical Society* **1998**, 145, 194; b) S. Komaba, T. Itabashi, T. Ohtsuka, H. Groult, N. Kumagai, B. Kaplan, H. Yashiro, *Journal of the Electrochemical Society* **2005**, 152, A937.

[38] D. P. Abraham, T. Spila, M. M. Furczon, E. Sammann, *Electrochem Solid St* **2008**, 11, A226.

[39] S. R. Gowda, K. G. Gallagher, J. R. Croy, M. Bettge, M. M. Thackeray, M. Balasubramanian, *Phys Chem Chem Phys* **2014**, 16, 6898.

[40] N. P. W. Pieczonka, Z. Y. Liu, P. Lu, K. L. Olson, J. Moote, B. R. Powell, J. H. Kim, *J Phys Chem C* **2013**, 117, 15947.

[41] J. Betz, J. P. Brinkmann, R. Nolle, C. Lurenbaum, M. Kolek, M. C. Stan, M. Winter, T. Placke, *Adv Energy Mater* **2019**, 9, 1900574.

[42] a) D. C. Lin, Y. Y. Liu, Y. Cui, *Nat Nanotechnol* **2017**, 12, 194; b) S. Li, M. W. Jiang, Y. Xie, H. Xu, J. Y. Jia, J. Li, *Adv Mater* **2018**, 30, 1706375.

[43] D. H. Jang, Y. J. Shin, S. M. Oh, *Journal of the Electrochemical Society* **1996**, 143, 2204.

[44] Y. Terada, Y. Nishiwaki, I. Nakai, F. Nishikawa, *Journal of Power Sources* **2001**, 97-8, 420.

[45] a) L. F. Wang, C. C. Ou, K. A. Striebel, J. J. S. Chen, *Journal of the Electrochemical Society* **2003**, 150, A905; b) Y. Y. Xia, Y. H. Zhou, M. Yoshio, *Journal of the Electrochemical Society* **1997**, 144, 2593; c) A. Blyr, A. Du Pasquier, G. Amatucci, J. M. Tarascon, *Ionics* **1997**, 3, 321; d) D. H. Jang, S. M. Oh, *Journal of the Electrochemical Society* **1997**, 144, 3342.

[46] a) Y. Shilina, B. Ziv, A. Meir, A. Banerjee, S. Ruthstein, S. Luski, D. Aurbach, I. C. Halalay, *Anal Chem* **2016**, 88, 4440; b) A. Banerjee, Y. Shilina, B. Ziv, J. M. Ziegelbauer, S. Luski, D. Aurbach, I. C. Halalay, *J Am Chem Soc* **2017**, 139, 1738.

[47] L. Hanf, J. Henschel, M. Diehl, M. Winter, S. Nowak, *Electrophoresis* **2020**, DOI 10.1002/elps.201900443.

[48] D. C. Tang, Y. Sun, Z. Z. Yang, L. B. Ben, L. Gu, X. J. Huang, *Chem Mater* **2014**, 26, 3535.

[49] X. Gao, Y. H. Ikuhara, C. A. J. Fisher, R. Huang, A. Kuwabara, H. Moriwake, K. Kohama, Y. Ikuhara, *J Mater Chem A* **2019**, 7, 8845.

[50] M. Hirayama, H. Ido, K. Kim, W. Cho, K. Tamura, J. Mizuki, R. Kanno, *J Am Chem Soc* **2010**, 132, 15268.

[51] M. M. Thackeray, *J Am Ceram Soc* **1999**, 82, 3347.

[52] D. Aurbach, M. D. Levi, K. Gamulski, B. Markovsky, G. Salitra, E. Levi, U. Heider, L. Heider, R. Oesten, *Journal of Power Sources* **1999**, 81, 472.

[53] a) A. Yamada, M. Tanaka, *Mater Res Bull* **1995**, 30, 715; b) A. Yamada, M. Tanaka, K. Tanaka, K. Sekai, *Journal of Power Sources* **1999**, 81, 73.

[54] M. M. Thackeray, Y. Shao-Horn, A. J. Kahaian, K. D. Kepler, J. T. Vaughey, S. A. Hackney, *Electrochem Solid St* **1998**, 1, 7.

[55] T. C. Liu, A. Dai, J. Lu, Y. F. Yuan, Y. G. Xiao, L. Yu, M. Li, J. Gim, L. Ma, J. J. Liu, C. Zhan, L. X. Li, J. X. Zheng, Y. Ren, T. P. Wu, R. Shahbazian-Yassar, J. G. Wen, F. Pan, K. Amine, *Nature Communications* **2019**, 10, 4721.

[56] M. X. Lin, L. B. Ben, Y. Sun, H. Wang, Z. Z. Yang, L. Gu, X. Q. Yu, X. Q. Yang, H. F. Zhao, R. Yu, M. Armand, X. J. Huang, *Chem Mater* **2015**, 27, 292.

[57] C. D. Amos, M. A. Roldan, M. Varela, J. B. Goodenough, P. J. Ferreira, *Nano Lett* **2016**, 16, 2899.

[58] S. Kim, M. Aykol, C. Wolverton, *Phys Rev B* **2015**, 92, 115411.

[59] Y. Y. Chen, L. B. Ben, B. Chen, W. W. Zhao, X. J. Huang, *Adv Mater Interfaces* **2018**, 5, 1800077.

[60] D. W. Shin, C. A. Bridges, A. Huq, M. P. Paranthaman, A. Manthiram, *Chem Mater* **2012**, 24, 3720.

[61] G. Zhou, X. Sun, Q. H. Li, X. Wang, J. N. Zhang, W. Yang, X. Yu, R. Xiao, H. Li, *J Phys Chem Lett* **2020**, 11, 3051.

[62] a) K. Leung, *Chem Mater* **2017**, 29, 2550; b) R. Benedek, M. M. Thackeray, J. Low, T. Bucko, *J Phys Chem C* **2012**, 116, 4050.

[63] a) D. Song, H. Ikuta, T. Uchida, M. Wakihara, *Solid State Ionics* **1999**, 117, 151; b) Y. S. Lee, N. Kumada, M. Yoshio, *Journal of Power Sources* **2001**, 96, 376; c) Y. Shin, A. Manthiram, *Chem Mater* **2003**, 15, 2954; d) Y. J. Shin, A. Manthiram, *Journal of the Electrochemical Society* **2004**, 151, A204; e) A. Gutierrez, A. Manthiram, *Journal of the Electrochemical Society* **2013**, 160, A901; f) L. L. Xiong, Y. L. Xu, T. Tao, J. B. Goodenough, *Journal of Power Sources* **2012**, 199, 214; g) S. Bhuvaneswari, U. V. Varadaraju, R. Gopalan, R. Prakash, *Electrochim Acta* **2019**, 301, 342.

[64] a) Y. Yu, M. W. Xiang, J. M. Guo, C. W. Su, X. F. Liu, H. L. Bai, W. Bai, K. J. Duan, *J Colloid Interf Sci* **2019**, 555, 64; b) C. Ma, L. Luo, K. W. Li, B. Zhou, Q. Shi, *Int J Electrochem Sc* **2019**, 14, 7643; c) Z. R. Yang, Y. J. Wang, X. C. Chen, H. Wu, Y. Zhang, *Chemistryselect* **2019**, 4, 9583.

[65] X. M. He, J. J. Li, Y. Cai, Y. W. Wang, H. R. Ying, C. Y. Jiang, C. R. Wan, *Solid State Ionics* **2005**, 176, 2571.

[66] J. L. Shi, D. D. Xiao, M. Y. Ge, X. Q. Yu, Y. Chu, X. J. Huang, X. D. Zhang, Y. X. Yin, X. Q. Yang, Y. G. Guo, L. Gu, L. J. Wan, *Adv Mater* **2018**, 30, 1705575.

[67] a) G. M. Liang, Z. B. Wu, C. Didier, W. C. Zhang, J. Cuan, B. H. Li, K. Y. Ko, P. Y. Hung, C. Z. Lu, Y. Z. Chen, G. Leniec, S. M. Kaczmarek, B. Johannessen, L. Thomsen, V. K. Peterson, W. K. Pang, Z. P. Guo, *Angew Chem Int Edit* **2020**; b) C. Locati, U. Lafont, L. Simonin, F. Ooms, E. M. Kelder, *Journal of Power Sources* **2007**, 174, 847; c) S. R. Li, C. H. Chen, J. R. Dahn, *Journal of the Electrochemical Society* **2013**, 160, A2166; d) J. Mao, M. Z. Ma, P. P. Liu, J. H. Hu, G. S. Shao, V. Battaglia, K. H. Dai, G. Liu, *Solid State Ionics* **2016**, 292, 70; e) M. Aklalouch, J. M. Amarilla, R. M. Rojas, I. Saadoune, J. M. Rojo, *Journal of Power Sources* **2008**, 185, 501; f) G. B. Zhong, Y. Y. Wang, Z. C. Zhang, C. H. Chen, *Electrochim Acta* **2011**, 56, 6554; g) H. L. Wang, T. A. Tan, P. Yang, M. O. Lai, L. Lui, *J Phys Chem C* **2011**, 115, 6102.

[68] a) J. G. Yang, X. P. Han, X. L. Zhang, F. Y. Cheng, J. Chen, *Nano Res* **2013**, 6, 679; b) R. Santhanam, B. Rambabu, *Journal of Power Sources* **2010**, 195, 5442.

[69] a) J. Lu, C. Zhan, T. P. Wu, J. G. Wen, Y. Lei, A. J. Kropf, H. M. Wu, D. J. Miller, J. W. Elam, Y. K. Sun, X. P. Qiu, K. Amine, *Nature Communications* **2014**, 5, 5693; b) J. Y. Piao, Y. G. Sun, S. Y. Duan, A. M. Cao, X. L. Wang, R. J. Xiao, X. Q. Yu, Y. Gong, L. Gu, Y. T. Li, Z. J. Liu, Z. Q. Peng, R. M. Qiao, W. L. Yang, X. Q. Yang, J. B. Goodenough, L. J. Wan, *Chem-Us* **2018**, 4, 1685; c) J. M. Lim, R. G. Oh, D. Kim, W. Cho, K. Cho, M. Cho, M. S. Park, *Chemsuschem* **2016**, 9, 2967; d) Y. Xue, L. L. Zheng, J. Wang, J. G. Zhou, F. D. Yu, G. J. Zhou, Z. B. Wang, *Acs Appl Energ Mater* **2019**, 2, 2982; e) W. Zhang, X. L. Sun, Y. X. Tang, H. R. Xia, Y. Zeng, L. Qiao, Z. Q. Zhu, Z. S. Lv, Y. Y. Zhang, X. Ge, S. B. Xi, Z. G. Wang, Y. H. Du, X. D. Chen, *J Am Chem Soc* **2019**, 141, 14038.

[70] a) Y. K. Sun, K. J. Hong, J. Prakash, *Journal of the Electrochemical Society* **2003**, 150, A970; b) M. M. Thackeray, C. S. Johnson, J. S. Kim, K. C. Lauzze, J. T. Vaughey, N. Dietz, D. Abraham, S. A. Hackney, W. Zeltner, M. A. Anderson, *Electrochem Commun* **2003**, 5, 752; c) J. S. Kim, C. S. Johnson, J. T. Vaughey, S. A. Hackney, K. A. Walz, W. A. Zeltner, M. A. Anderson, M. M. Thackeray, *Journal of the Electrochemical Society* **2004**, 151, A1755; d) S. C. Park, Y. M. Kim, S. C. Han, S. Ahn, C. H. Ku, J. Y. Lee, *Journal of Power Sources* **2002**, 107, 42.

[71] a) A. Tron, Y. D. Park, J. Mun, *Journal of Power Sources* **2016**, 325, 360; b) J. N. Cao, G. S. Cao, H. M. Yu, J. A. Xie, X. B. Zhao, *Rare Metals* **2011**, 30, 39; c) S. Zhao, Y. Bai, Q. Chang, Y. Yang, W. Zhang, *Electrochim Acta* **2013**, 108, 727.

[72] a) C. B. Qing, Y. Bai, J. M. Yang, W. F. Zhang, *Electrochim Acta* **2011**, 56, 6612; b) D. Q. Liu, Z. Z. He, X. Liu, *Mater Lett* **2007**, 61, 4703.

[73] R. Zhao, L. Li, T. H. Xu, D. D. Wang, D. Pan, G. J. He, H. L. Zhao, Y. Bai, *Acs Appl Mater Inter* **2019**, 11, 16233.

[74] R. Vidu, P. Stroeve, *Ind Eng Chem Res* **2004**, 43, 3314.

[75] L. Li, R. Zhao, D. Pan, S. Yi, L. Gao, G. He, H. Zhao, C. Yu, Y. Bai, *Journal of Power Sources* **2020**, 450, 227677.

[76] a) D. K. Kim, P. Muralidharan, H. W. Lee, R. Ruffo, Y. Yang, C. K. Chan, H. Peng, R. A. Huggins, Y. Cui, *Nano Lett* **2008**, 8, 3948; b) K. Zhang, X. P. Han, Z. Hu, X. L. Zhang, Z. L. Tao, J. Chen, *Chem Soc Rev* **2015**, 44, 699.

[77] a) H. Yamane, T. Inoue, M. Fujita, M. Sano, *Journal of Power Sources* **2001**, 99, 60; b) K. Amine, J. Liu, S. Kang, I. Belharouak, Y. Hyung, D. Vissers, G. Henriksen, *Journal of Power Sources* **2004**, 129, 14; c) S. S. Zhang, *Journal of Power Sources* **2006**, 162, 1379; d) S. S. Zhang, K. Xu, T. R. Jow, *J Solid State Electr* **2003**, 7, 492; e) A. Banerjee, B. Ziv, Y. Shilina, S. Luski, D. Aurbach, I. C. Halalay, *Acs Energy Lett* **2017**, 2, 2388.

[78] a) L. M. Suo, O. Borodin, T. Gao, M. Olguin, J. Ho, X. L. Fan, C. Luo, C. S. Wang, K. Xu, *Science* **2015**, 350, 938; b) X. L. Fan, L. Chen, O. Borodin, X. Ji, J. Chen, S. Hou, T. Deng, J. Zheng, C. Y. Yang, S. C. Liou, K. Amine, K. Xu, C. S. Wang, *Nat Nanotechnol* **2018**, 13, 715; c) W. Xue, Z. Shi, M. Huang, S. Feng, C. Wang, F. Wang, J. Lopez, B. Qiao, G. Xu, W. Zhang, Y. Dong, R. Gao, Y. Shao-Horn, J. A. Johnson, J. Li, *Energ Environ Sci* **2020**, 13, 212.

[79] L. Chen, J. Zhang, Q. Li, J. Vatamanu, X. Ji, T. P. Pollard, C. Cui, S. Hou, J. Chen, C. Yang, L. Ma, M. S. Ding, M. Garaga, S. Greenbaum, H.-S. Lee, O. Borodin, K. Xu, C. Wang, *Acs Energy Lett* **2020**, 5, 968.

[80] L. M. Suo, W. J. Xue, M. Gobet, S. G. Greenbaum, C. Wang, Y. M. Chen, W. L. Yang, Y. X. Li, J. Li, *P Natl Acad Sci USA* **2018**, 115, 1156.

[81] a) L. B. Hu, Z. C. Zhang, K. Amine, *Electrochem Commun* **2013**, 35, 76; b) X. Cao, X. He, J. Wang, H. D. Liu, S. Roser, B. R. Rad, M. Evertz, B. Streipert, J. Li, R. Wagner, M. Winter, I. Cekic-Laskovic,

Acs Appl Mater Inter **2016**, 8, 25971.

[82] a) Y. Uchimoto, K. Arnezawa, T. Furushita, M. Wakihara, I. Taniguchi, *Solid State Ionics* **2005**, 176, 2377; b) M. Z. Liu, B. Y. Jin, Q. H. Zhang, X. L. Zhan, F. Q. Chen, *J Alloy Compd* **2018**, 742, 619; c) G. Homann, L. Stolz, J. Nair, I. C. Laskovic, M. Winter, J. Kasnatscheew, *Sci Rep* **2020**, 10, 4390.

[83] J. H. Zhao, J. J. Zhang, P. Hu, J. Ma, X. G. Wang, L. P. Yue, G. J. Xu, B. S. Qin, Z. H. Liu, X. H. Zhou, G. L. Cui, *Electrochim Acta* **2016**, 188, 23.

[84] a) H. Kitaura, A. Hayashi, K. Tadanaga, M. Tatsumisago, *Journal of the Electrochemical Society* **2010**, 157, A407; b) H. Kitaura, A. Hayashi, K. Tadanaga, M. Tatsumisago, *Solid State Ionics* **2011**, 192, 304; c) S. Yubuchi, Y. Ito, T. Matsuyama, A. Hayashi, M. Tatsumisago, *Solid State Ionics* **2016**, 285, 79.

[85] G. Oh, M. Hirayama, O. Kwon, K. Suzuki, R. Kanno, *Chem Mater* **2016**, 28, 2634.

[86] a) L. Miara, A. Windmuller, C. L. Tsai, W. D. Richards, Q. L. Ma, S. Uhlenbruck, O. Guillon, G. Ceder, *Acs Appl Mater Inter* **2016**, 8, 26842; b) X. G. Liu, J. Tan, J. Fu, R. X. Yuan, H. Wen, C. H. Zhang, *Acs Appl Mater Inter* **2017**, 9, 11696.

[87] a) J. B. Bates, G. R. Gruzalski, N. J. Dudney, C. F. Luck, X. H. Yu, *Solid State Ionics* **1994**, 70, 619; b) M. Baba, N. Kumagai, N. Fujita, K. Ohta, K. Nishidate, S. Komaba, H. Groult, D. Devilliers, B. Kaplan, *Journal of Power Sources* **2001**, 97-8, 798; c) J. Schwenzel, V. Thangadurai, W. Weppner, *Journal of Power Sources* **2006**, 154, 232; d) C. Yada, A. Ohmori, K. Ide, H. Yamasaki, T. Kato, T. Saito, F. Sagane, Y. Iriyama, *Adv Energy Mater* **2014**, 4, 1301416; e) J. C. Li, C. Ma, M. F. Chi, C. D. Liang, N. J. Dudney, *Adv Energy Mater* **2015**, 5, 1401408; f) L. Li, S. Liu, H. Zhou, Q. Lei, K. Qian, *Mater Lett* **2018**, 216, 135.

[88] S. Kim, M. Hirayama, K. Suzuki, R. Kanno, *Solid State Ionics* **2014**, 262, 578.

[89] P. Y. Xu, W. Rheinheimer, S. N. Shuvo, Z. M. Qi, O. Levit, H. Y. Wang, Y. Ein-Eli, L. A. Stanciu, *Chemelectrochem* **2019**, 6, 4576.

[90] Wikipedia, Spinel group, https://en.wikipedia.org/wiki/Spinel_group, accessed: Feb 20, 2020.

[91] A. Jain, S. P. Ong, G. Hautier, W. Chen, W. D. Richards, S. Dacek, S. Cholia, D. Gunter, D. Skinner, G. Ceder, K. A. Persson, *Apl Mater* **2013**, 1, 011002.

[92] a) J. R. Dahn, E. W. Fuller, M. Obrovac, U. Vonsacken, *Solid State Ionics* **1994**, 69, 265; b) R. Kanno, H. Kubo, Y. Kawamoto, T. Kamiyama, F. Izumi, Y. Takeda, M. Takano, *J Solid State Chem* **1994**, 110, 216.

[93] D. Liu, W. Zhu, J. Trottier, C. Gagnon, F. Barray, A. Guerfi, A. Mauger, H. Groult, C. M. Julien, J. B. Goodenough, K. Zaghi, *Rsc Adv* **2014**, 4, 154.

[94] W. D. Li, B. H. Song, A. Manthiram, *Chem Soc Rev* **2017**, 46, 3006.

[95] G. Hautier, A. Jain, S. P. Ong, B. Kang, C. Moore, R. Doe, G. Ceder, *Chem Mater* **2011**, 23, 3495.

[96] J. Song, D. W. Shin, Y. H. Lu, C. D. Amos, A. Manthiram, J. B. Goodenough, *Chem Mater* **2012**, 24, 3101.

[97] a) D. H. Seo, J. Lee, A. Urban, R. Malik, S. Kang, G. Ceder, *Nat Chem* **2016**, 8, 692; b) G. Assat, J. M. Tarascon, *Nature Energy* **2018**, 3, 373.

[98] H. F. Wang, Y. I. Jang, B. Y. Huang, D. R. Sadoway, Y. T. Chiang, *Journal of the Electrochemical Society* **1999**, 146, 473.

[99] R. Yazami, Y. Ozawa, H. Gabrisch, B. Fultz, *Electrochim Acta* **2004**, 50, 385.

[100] J. Kikkawa, S. Terada, A. Gunji, T. Nagai, K. Kurashima, K. Kimoto, *J Phys Chem C* **2015**, 119, 15823.

[101] H. Y. Tan, S. Takeuchi, K. K. Bharathi, I. Takeuchi, L. A. Bendersky, *Acs Appl Mater Inter* **2016**, 8,

6727.

[102] A. Yano, M. Shikano, A. Ueda, H. Sakaebe, Z. Ogumi, *Journal of the Electrochemical Society* **2017**, 164, A6116.

[103] W. M. Seong, K. Yoon, M. H. Lee, S. K. Jung, K. Kang, *Nano Lett* **2019**, 19, 29.

[104] K. W. Nam, S. M. Bak, E. Y. Hu, X. Q. Yu, Y. N. Zhou, X. J. Wang, L. J. Wu, Y. M. Zhu, K. Y. Chung, X. Q. Yang, *Adv Funct Mater* **2013**, 23, 1047.

[105] S. K. Jung, H. Gwon, J. Hong, K. Y. Park, D. H. Seo, H. Kim, J. Hyun, W. Yang, K. Kang, *Adv Energy Mater* **2014**, 4, 1300787.

[106] F. Lin, I. M. Markus, D. Nordlund, T. C. Weng, M. D. Asta, H. L. L. Xin, M. M. Doeff, *Nature Communications* **2014**, 5, 3529.

[107] H. Kim, M. G. Kim, H. Y. Jeong, H. Nam, J. Cho, *Nano Lett* **2015**, 15, 2111.

[108] J. Hong, D. H. Seo, S. W. Kim, H. Gwon, S. T. Oh, K. Kang, *J Mater Chem* **2010**, 20, 10179.

[109] A. Ito, K. Shoda, Y. Sato, M. Hatano, H. Horie, Y. Ohsawa, *Journal of Power Sources* **2011**, 196, 4785.

[110] B. Xu, C. R. Fell, M. F. Chi, Y. S. Meng, *Energ Environ Sci* **2011**, 4, 2223.

[111] M. Gu, I. Belharouak, J. M. Zheng, H. M. Wu, J. Xiao, A. Genc, K. Amine, S. Thevuthasan, D. R. Baer, J. G. Zhang, N. D. Browning, J. Liu, C. M. Wang, *Acs Nano* **2013**, 7, 760.

[112] J. M. Zheng, P. H. Xu, M. Gu, J. Xiao, N. D. Browning, P. F. Yan, C. M. Wang, J. G. Zhang, *Chem Mater* **2015**, 27, 1381.

[113] P. F. Yan, A. M. Nie, J. M. Zheng, Y. G. Zhou, D. P. Lu, X. F. Zhang, R. Xu, I. Belharouak, X. T. Zu, J. Xiao, K. Amine, J. Liu, F. Gao, R. Shahbazian-Yassar, J. G. Zhang, C. M. Wang, *Nano Lett* **2015**, 15, 514.

[114] P. F. Yan, J. M. Zheng, Z. K. Tang, A. Devaraj, G. Y. Chen, K. Amine, J. G. Zhang, L. M. Liu, C. M. Wang, *Nat Nanotechnol* **2019**, 14, 602.

[115] S. M. Bak, E. Y. Hu, Y. N. Zhou, X. Q. Yu, S. D. Senanayake, S. J. Cho, K. B. Kim, K. Y. Chung, X. Q. Yang, K. W. Nam, *Acs Appl Mater Inter* **2014**, 6, 22594.

[116] a) S. H. Park, S. H. Kang, C. S. Johnson, K. Amine, M. M. Thackeray, *Electrochem Commun* **2007**, 9, 262; b) J. R. Croy, J. S. Park, Y. Shin, B. T. Yonemoto, M. Balasubramanian, B. R. Long, Y. Ren, M. M. Thackeray, *Journal of Power Sources* **2016**, 334, 213.

[117] a) Y. Cho, S. Lee, Y. Lee, T. Hong, J. Cho, *Adv Energy Mater* **2011**, 1, 821; b) F. Wu, N. Li, Y. F. Su, L. J. Zhan, L. Y. Bao, J. Wang, L. Chen, Y. Zheng, L. Q. Dai, J. Y. Peng, S. Chen, *Nano Lett* **2014**, 14, 3550; c) J. H. Shim, K. S. Lee, A. Missyul, J. Lee, B. Linn, E. C. Lee, S. Lee, *Chem Mater* **2015**, 27, 3273; d) P. Oh, B. H. Song, W. D. Li, A. Manthiram, *J Mater Chem A* **2016**, 4, 5839; e) X. D. Zhang, J. L. Shi, J. Y. Liang, Y. X. Yin, J. N. Zhang, X. Q. Yu, Y. G. Guo, *Adv Mater* **2018**, 30, 1801751.

[118] Z. Q. Rong, R. Malik, P. Canepa, G. S. Gautam, M. Liu, A. Jain, K. Persson, G. Ceder, *Chem Mater* **2015**, 27, 6016.

[119] a) B. J. Johnson, D. H. Doughty, J. A. Voigt, T. J. Boyle, *Journal of Power Sources* **1997**, 68, 634; b) M. Y. Saidi, J. Barker, R. Koksbang, *J Solid State Chem* **1996**, 122, 195; c) M. Wakihara, G. H. Li, H. Ikuta, T. Uchida, *Solid State Ionics* **1996**, 86-8, 907; d) F. Cao, J. Prakash, *Electrochim Acta* **2002**, 47, 1607; e) H. J. Bang, V. S. Donepudi, J. Prakash, *Electrochim Acta* **2002**, 48, 443; f) A. Ito, D. Li, Y. Lee, K. Kobayakawa, Y. Sato, *Journal of Power Sources* **2008**, 185, 1429; g) A. Veluchamy, H. Ikuta, M. Wakihara, *Solid State Ionics* **2001**, 143, 161; h) K. M. Shaju, G. V. S. Rao, B. V. R. Chowdari, *J Mater Chem* **2003**, 13, 106; i) D. Kovacheva, B. Markovsky, G. Salitra, Y. Talyosef, M. Gorova, E. Levi, M. Riboch, H. J. Kim, D. Aurbach, *Electrochim Acta* **2005**, 50, 5553; j) H. Xia, Y. S. Meng, L.

Lu, G. Ceder, *Journal of the Electrochemical Society* **2007**, 154, A737; k) M. Park, X. C. Zhang, M. D. Chung, G. B. Less, A. M. Sastry, *Journal of Power Sources* **2010**, 195, 7904; l) R. Amin, I. Belharouak, *Journal of Power Sources* **2017**, 348, 318.

[120] X. H. Ma, B. Kang, G. Ceder, *Journal of the Electrochemical Society* **2010**, 157, A925.

[121] M. J. Lee, E. Lho, P. Bai, S. Chae, J. Li, J. Cho, *Nano Lett* **2017**, 17, 3744.

[122] a) T. Yuan, Z. P. Tan, C. R. Ma, J. H. Yang, Z. F. Ma, S. Y. Zheng, *Adv Energy Mater* **2017**, 7; b) S. T. Wang, Y. Yang, Y. H. Dong, Z. T. Zhang, Z. L. Tang, *J Adv Ceram* **2019**, 8, 1601625, 1.

[123] S. T. Wang, W. Quan, Z. Zhu, Y. Yang, Q. Liu, Y. Ren, X. Y. Zhang, R. Xu, Y. Hong, Z. T. Zhang, K. Amine, Z. L. Tang, J. Lu, J. Li, *Nature Communications* **2017**, 8, 627.

[124] W. Zhang, D. H. Seo, T. Chen, L. J. Wu, M. Topsakal, Y. M. Zhu, D. Y. Lu, G. Ceder, F. Wang, *Science* **2020**, 367, 1030.

[125] A. Urban, J. Lee, G. Ceder, *Adv Energy Mater* **2014**, 4, 1400478.

[126] J. Lee, D. A. Kitchaev, D. H. Kwon, C. W. Lee, J. K. Papp, Y. S. Liu, Z. Y. Lun, R. J. Clement, T. Shi, B. D. McCloskey, J. H. Guo, M. Balasubramanian, G. Ceder, *Nature* **2018**, 556, 185.